DYNAMIC CONTACT ANGLES AND WETTING FRONT INSTABILITY IN SOILS

A Thesis

Presented to the Faculty of the Graduate School

of Cornell University

in Partial Fulfillment of the Requirements for the Degree of

Masters of Science

by

Christine E. Baver

January 2013

ABSTRACT

Dynamic contact could provide a mechanism for initiating the instability of wetting fronts and the formation of gravity fingers/columns in porous media. To study those dynamic contact angles when gravity effects are present, rectangular capillary tubes are used to facilitate the observation of the complete interface without geometric distortion. Results show that if the dynamic contact angle minus the static contact angle is used, we obtain good agreement with previous observations. In addition, we show that in our experiments, unlike previous observations, contact angles are independent of capillary size. It also points out a way to calculate the capillary pressure at the wetting front as a function of the flux in the finger and grain size diameter.

BIOGRAPHICAL SKETCH

Christine was born in Lancaster, PA and grew up in Mercer, PA. In 2009, she completed her undergraduate studies in physics at Pacific Lutheran University. She became interested in environmental engineering through a hydrology course during study abroad experience in Scotland in the Fall of 2007. She gained some experience with environmental engineering through a summer internship with the US Army Corps of Engineers working with weirs, invasive species and ArcGIS. In 2009, she enrolled at Cornell University to study environmental engineering with Tammo Steenhuis.

ACKNOWLEDGEMENTS

I want to thank Tammo Steenhuis, Jean-Yves Parlange for the privilege and opportunity to work with them and for their continued patience and persistence with me during my studies. I would also like to thank Cathelijne Stoof for her valuable insight, comments and friendship. Members of the Soil and Water Lab have been invaluable to me, especially Veronica Morales, Sheila Saia and Christian Guzman for their presence, suggestions and kindness during the years. I also want to thank the individuals in the Cornell Wushu Club, Stewart Little Coop and Graduate Christian Fellowship for giving me countless opportunities to have fun and relax. I would also like to thank the administrative staff of the Biological and Environmental Engineering Department at Cornell for their guidance during paperwork and overall encouragement. I also want to thank my physics professors at Pacific Lutheran University, Bogomil Gerganov, Rich Louie, Steven Starkovich, Katrina Hay, William Greenwood and Kwong-Tin Tang and classmates at Pacific Lutheran for introducing me to the world of physics and providing opportunities to pursue research. I also wish to thank my parents for being my biggest advocate growing up to make sure I was in regular classrooms and integrated into all of the activities with my peers. I would like to thank Victor Wang for his endless encouragement and understanding patience. And finally, I wish to thank Doug Caveney for building the adjustable apparatus and Binational Agricultural Research and Development Fund (BARD), Project No. IS-3962- 07 for their financial assistance.

TABLE OF CONTENTS

BIOGRAPHICAL SKETCH iii

ACKNOWLEDGEMENTS iv

LIST OF FIGURES vii

LIST OF TABLES ix

LIST OF SYMBOLS x

SECTION 1 1

Introduction

SECTION 2 3

Hoffman's Shift Factor and Jiang's equation

SECTION 3 5

Materials and Methods

SECTION 4 10

Results and Discussion

SECTION 5 16

Conclusion

APPENDIX A 18

Cleaning Procedure of Capillary Tubes

APPENDIX B 19

Additional Dimensionless Numbers

APPENDIX C 21

Static Contact Angle of Glycerin

APPENDIX D 22

Brief Mathematical Background

APPENDIX E 28

Additional Graphs and Tables

REFERENCES 46

LIST OF FIGURES

Figure 1 4
Hoffman's [1975] experimental data (points) with the fitted approximation by Jiang [1979] (line).

Figure 2 7
a) Experimental setup comprising of an adjustable apparatus stand with a capillary tube (A), see detail in 2b), mounted on a stand (B), and a bright-field microscope (C) connected to a personal computer that displays the image (D). Adjustable apparatus stand (2b, 2c) is composed of a platform with an adjustable arm (F) which position can be changed and fixed to a required inclination using a thumb screw (G) and a protractor or inclination scale (H) mounted behind the adjustable arm.

Figure 3 9
Protractor method measurement of contact angle (θ_a) in a capillary, with lines drawn (XYZ) for calculation of the contact angle; and 3b) apex method of measuring contact angle that uses the Cartesian coordinate values of the point where the liquid, capillary tube and air meet (A, B) and the position where the liquid and air intersect at the radius of the capillary (C).

Figure 4 11
Froude vs. Reynolds Number (n=334) for 5 different liquids and 4 chamber sizes, in which red squares indicate experimental results that followed Poiseuille's Law, and blue diamonds that did not. A linear regression line is fitted (R^2=0.99).

Figure 5 13
a) All experiment results plotted with dynamic contact angle as a function of capillary number with the results of Hoffman (1975), R^2 = 0.63, b) The best fit line for the glycerin data is plotted with our $\theta_s = 0°$ line from our experiment data and Jiang's correction(eqn. 2) based on our $\theta_s = 0°$ line using θ_s as 34° as a function of capillary number, c) All experiment results are plotted as a reduced dynamic contact angles; $\theta_{\text{Reduced}} = \frac{\theta_m - \theta_s}{(180 - \theta_s)} * 180$ as a function of capillary number; R^2=0.86 with an average curve.

Figure 6 15
Comparison of apex-contact line method and protractor method on non-circular interfaces. Image A is a 3.5-9 mm chamber, image B is 3.85-11.95 mm chamber.

Figure D1 ` 25
Dynamic contact angle of V100000 silicon oil on rectangular capillary tube. Solid curve: Hydrodynamic theory, eq (10), ln(L/Lm) = 9.3. Dashed curve: MKT, eq (11), λ = .80 nm, and k^0 = 2300 and θ_s = 0 in both cases.

Figure D2 25
Dynamic contact angle of V30000 silicon oil on rectangular capillary tube. Solid curve: Hydrodynamic theory, eq (10), ln(L/Lm) = 9.1. Dashed curve: MKT, eq (11), λ = .80 nm, and k^0 = 7000 and θ_s = 0 in both cases.

Figure D3 26
Dynamic contact angle of V500 silicon oil on rectangular capillary tube. Solid curve: Hydrodynamic theory, eq (10), ln(L/Lm) = 12.8. Dashed curve: MKT, eq (11), λ = .80 nm, and k^0 = 221098 and θ_s = 0 in both cases.

Figure D4 26
Dynamic contact angle of V100 silicon oil on rectangular capillary tube. Solid curve: Hydrodynamic theory, eq (10), ln(L/Lm) = 9.4. Dashed curve: MKT, eq (11), λ = .80 nm, and k^0 = 185000 and θ_s = 0 in both cases.

Figure D5 27
Dynamic contact angle of glycerin on rectangular capillary tube. Solid curve: Hydrodynamic theory, eq (10), ln(L/Lm) = 20 and θ_s= 50. Dashed curve: MKT, eq (11), $\lambda = 6*10^{-10}$ nm, and k^0 = 250000 and θ_s = 50.

Figure E1.....29
Experimental Results plotted as a function of Reynolds number.

Figure E2.....29
Experimental Results plotted as a function of Bond Number.

Figure E3.....30
Experimental Results plotted as a function of Weber Number.

LIST OF TABLES

Table 1 5
Summary of Liquid Properties. Values are averages over the replicates of the measurement (n=3) ± one standard deviation.

Table 2 10
Experimental design, showing the number of replicates (n) performed for the different combinations of liquid type (order based on increasing viscosity) and chamber size.

Table E1 28
Replicates In the case of V100000 and V30000 fluid, the meniscus began to deviate from a circular shape and approached a parabolic profile at high inclinations indicated with an X.

Table E2 31
All experiment data.

LIST OF SYMBOLS

μ	viscosity of the liquid	Pa*s
v	contact line velocity	m/s
γ	surface or interfacial tension	N/m
ρ	density of the fluid	g/ml
r	characteristic length (radius)	m
g	gravitational acceleration	m/s^2
θ_D	dynamic contact angle	degrees
θ_s	static contact angle	degrees
l	characteristic length	m
L	macroscopic length scale	micrometers
Lm	microscopic length scales	micrometers
k^0	equilibrium frequency of the random molecular displacements occurring within three phase zone	1/s
λ	average distance of each displacement	nm
k_B	Boltzmann's constant	m^2kg/s^2K
T	temperature	Kelvin

1. Introduction

While many experiments have been conducted to study unstable flow, questions remain. Early research by Saffman and Taylor [1958] and Chuoke *et al.* [1959] primarily focused on viscous fingering. Later field observations by Bond [1964] and experiments of Hill and Parlange [1972] focused on gravity fingering, or column flow, where viscosity is less important; see also the observations of Raats [1973]. Column flows are the most prevalent mechanism in nature to rapidly transport large quantities of water downward, bypassing most of the soil matrix [*Starr et al.*, 1978]. The main difficulty in understanding column flow is that moisture content within these columns is not uniformly distributed (columns are wetter at the tip) and that the wetting takes place within only a few pores. Because Richards' equation assumes that changes take place over the Darcy scale, it cannot be used reliably to estimate derivatives on these short pore-scale distances. Trying to correct Richards' equation by adding higher order derivatives as is sometimes considered cannot improve the validity of the equation. Even though Richards' equation cannot be used to analyze processes occurring at the tip of the wetting front, it adequately describes the structure of column flow far enough from the tip. For instance, the decreasing water content with the distance from the tip [*Selker et al.*, 1992] and the width of the column flow [*Parlange and Hill*, 1976] can both be obtained with Richards' equation. While Parlange and Hill [1976] originally assumed that the tip of the column was saturated, this is neither true in general nor necessary [*Hillel and Baker*, 1988; *Liu et al.*, 1995]. An accepted theory to predict the water content at the tip does not exist and therefore in many applications the experimentally observed moisture content is used [*Liu et al.*, 1995; *Aminzadeh et al.*, 2011]. We pose that a dynamic contact angle greater than the static contact angle, could provide an explanation for the different observed moisture contents at the wetting front.

The dynamic contact angle is the angle between the moving interface where the liquid/vapor interface and solid surface meet. Dynamic contact angles and dynamic wetting affect processes such as solute transport in soil [*Jarvis et al.*, 1991; *Jarvis*, 2007], ink printing [*Clarke et al.*, 2002; *van Dam and Le Clerc*, 2004] and protein absorption [*Stadler et al.*, 2003; *Velzenberger et al.*, 2009].

Hoffman [1975] carried out the first fundamental experiment involving the dependence of the dynamic contact angle on velocity using slugs of liquid. The observed angle is sometimes called "apparent," as some authors [*Hansen and Toong*, 1971a; *Ngan and Dussan V.*, 1982] speculate that the contact angle is static at microscale, however we here focus on the macro scale contact angle and ignore that fine point. Hoffman's [1975] physical results have been confirmed by other researchers [*Rose and Heins*, 1962; *Hansen and Toong*, 1971b; *Tanner*, 1979; *Legait and Sourieau*, 1985].

Much experimental work has been done with transparent circular capillary tubes to mimic a soil pore [*Huh and Mason*, 1977; *Tsai and Miksis*, 1994] or for industrial purposes [*Stroup et al.*, 1969; *da Silva et al.*, 2009; *Zhang and Balcom*, 2010]. Experimental studies with slug flow include horizontal capillary tubes [*Legait and Sourieau*, 1985], self-propelling slugs [*Bico and Quéré*, 2002], and included symmetric and asymmetric features on a surface on horizontal capillaries [*Extrand*, 2007].

Flow in rectangular chambers is also of interest for industrial purposes [*Lee et al.*, 2005; *Taha and Cui*, 2006] and rectangular tubes are more suitable to mimic porous media because liquid is often retained in corners [*Blunt et al.*, 1995; *Spildo and Buckley*, 1999; *Taha and Cui*, 2006]. Gravity driven slug flow in circular capillary tubes has been investigated by Bico and

Quéré, [2001] and Lunati and Or, [2009]. There is no experimental data for slug flow driven by gravity in rectangular chambers. More importantly, rectangular capillary tubes are used because the surface distortion of the interface is minimal.

2. Hoffman's Shift Factor and Jiang's equation

When dealing with slug flow, four key factors can play a major role: gravity, viscosity, surface tension, and inertia. Those are quantified using dimensionless numbers. The capillary number (*Ca*) comparing viscous force to surface tension is defined as:

$$Ca = \mu v / \gamma \tag{1}$$

where μ is the viscosity of the liquid (Pa•s), V is a contact line velocity (m/s), and γ is the surface tension (N/m) between the two fluid phases. Hoffman [1975] preformed his experiments with horizontal capillary tubes using a steel plunger and five liquids. Since the tubes were placed horizontally, effects of gravity did not enter. From two silicon liquids with a static contact angle of zero (GE and Brookfield), Hoffman [1975] plotted dynamic contact angles (ranging from 0 to 180°) as a function of capillary number. Because the dynamic contact angle – capillary number relationships found for other liquids (Dow Corning fluid, Admex and Santicizer, with non-zero static contact angles of 12°, 69° and 67°, respectively) did not match the initial curve, he used a "shift" correction to match the results. This shift factor was found by looking up the capillary number corresponding to the liquid's static contact angle (in the initial curve), and adding this value to the measured capillary values. The resulting graph in which all liquids fit one curve is presented in Fig. 1, in which all points were fitted with an equation introduced by Jiang [1979]:

$$\frac{\cos\theta_s - \cos\theta_m}{\cos\theta_s + 1} = \tanh\left(4.96\ Ca^{.702}\right) \quad (2)$$

where θ_s is the static contact angle and θ_m is the measured contact angle. For simplicity, Jiang's [1979] curve with θ_s equal to zero will be used to depict Hoffman's curve in the rest of the paper to compare with our results.

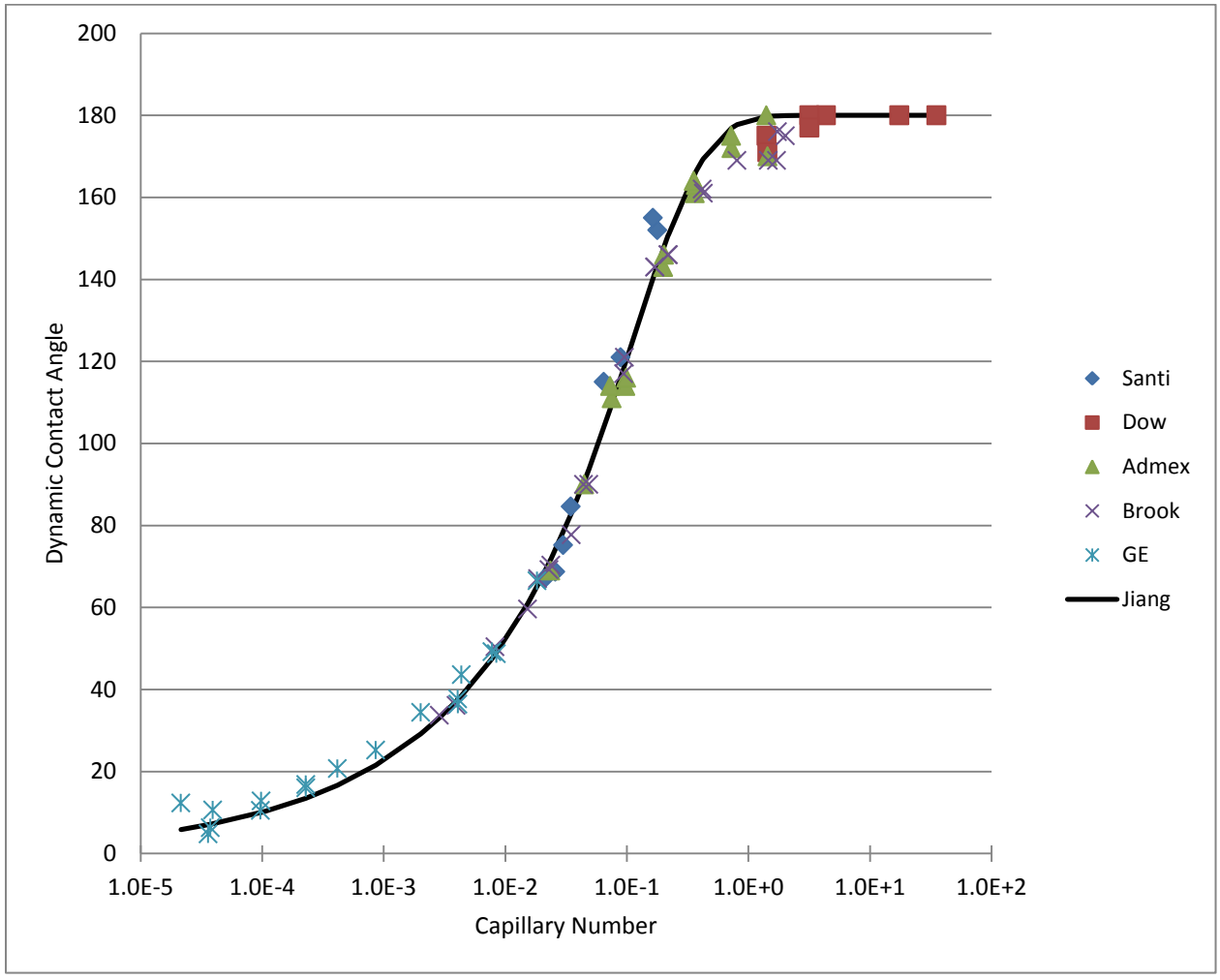

Figure 1: Hoffman's [1975] experimental data (points) with the fitted approximation by Jiang [1979] (line).

3. Materials and Methods

3.1 Materials

We have performed experiments with glycerin and different silicon liquids of variable viscosity in different size rectangular capillary tubes. The rectangular tubes used in these experiments were 20-60 cm long rectangular borosilicate glass tubes (Friedrich & Dimmock Inc., Millville, NJ, USA) of four different dimensions: 2 x 4 mm, 2 x 6 mm, 3.5 x 9 mm, and 3.85 x 11.95 mm. Five liquids were tested: four silicones (Brookfield Engineering Laboratories Inc., Middleboro, MA, USA) selected to cover a range of viscosities, and glycerol (*Mallinckrodt,* Paris, KY, USA) (Table 1). The static contact angle of the silicon liquids was 0 degrees in agreement with Hoffman [1975] and Fermigier and Jenffer [1991]. The static contact angle of glycerin was measured to be 34 degrees following the static sessile drop/goniometer method [*Shang et al.,* 2008].

Table 1: Summary of Liquid Properties. Values are averages over the replicates of the measurement (n=3) ± one standard deviation.

Manufacturer	Liquid	Viscosity (Pa•s)	Surface tension (N/m)	Density (kg/m^3)	Static contact angle (°)
Dow Corning	Glycerin	1.34±0	0.0640±0.002	1254±4	34±3
Brookfield Standard	V100000	104.32*	0.0225±0.002	999±4	0
Brookfield Standard	V30000	30.88*	0.0226±0.002	1002±15	0
Brookfield Standard	V500	0.486*	0.0240±0.002	975±12	0
Brookfield Standard	V100	0.0968*	0.0227±0.002	966±4	0

*supplied by manufacturer

Viscosity was measured with a SV-10 Vibro Viscometer (Worcestershire, UK); surface tension was measured with a Fisher Surface Tensiomat (Model 21, Fisher Scientific, Pittsburgh, PA, USA) and fluid density was measured by weighing a known volume of liquid.

3.2 Experimental setup

The shape of the moving interface was captured through a Hirox-Digital KH-7700 bright field microscope (Hirox-USA, River Edge, NJ, USA) mounted with a MX-5040SZ Mid-Range Straight Zoom lens and AD-5040LOWRS Low Magnification Rotary-Head adaptor, and connected to a personal computer (Fig. 2a). Because the microscope had a maximum recording speed of 30 frames/sec, the greatest fluid velocity that could be captured was ~1 cm/s. Results were obtained by using recording speeds between 30 frames/sec and 20 frames/min. To vary the strength of gravitational force, a platform with an adjustable apparatus was designed to support capillary tubes at different specific inclinations (Fig. 2b). A built-in protractor, made of thick transparent acrylic, allowed the apparatus to be adjusted for inclination values between 0° and 90°, while a small white piece of paper placed on the apparatus arm provided a white background and reduced light reflection or image distortion from the acrylic material. The setup was designed such that air could move freely and unobstructed at both ends of the capillary and the apparatus was secured using a thumb screw and stage clips. To allow for microscope images be taken at a 90° angle with the capillary, the microscope was tilted to offset the inclination of the capillary tube (Fig. 2c).

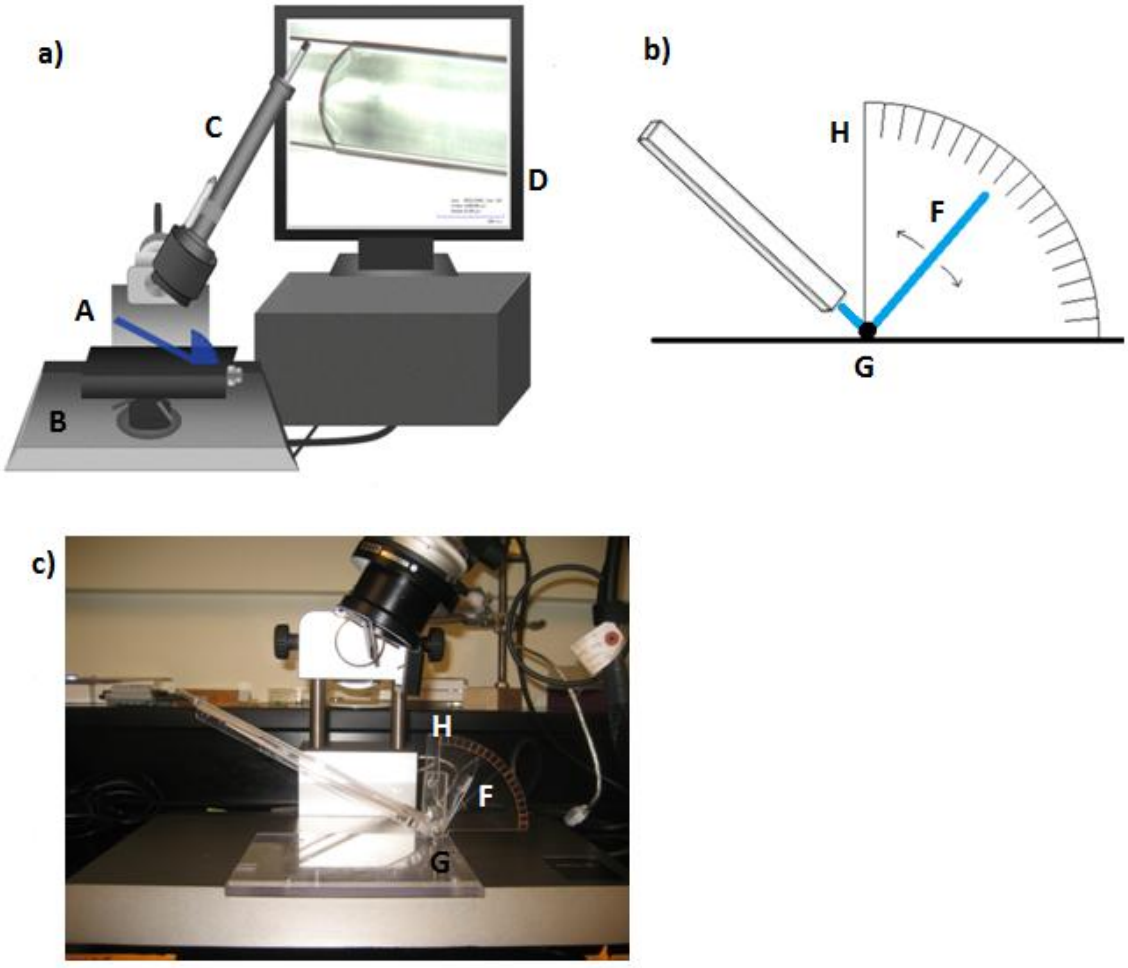

Figure 2a): Experimental setup comprising of an adjustable apparatus stand with a capillary tube (A), see detail in 2b), mounted on a stand (B), and a bright-field microscope (C) connected to a personal computer that displays the image (D). Adjustable apparatus stand (2b, 2c) is composed of a platform with an adjustable arm (F) which position can be changed and fixed to a required inclination using a thumb screw (G) and a protractor or inclination scale (H) mounted behind the adjustable arm.

3.3 Experimental procedure

At the start of each experiment, a slug of liquid between 150 and 3000 µl was pipetted into a horizontally-placed capillary tube. The slugs were long enough to ensure that the velocity would remain constant and follow Poiseuille's law. After the slug was inserted into the capillary tube, the two ends of the tube were capped to minimize premature sliding movement of the liquid within as it was placed on the apparatus. At the desired inclination, the slug was then allowed to move down the capillary tube.

After the initial transition period, when the wetting front had traveled 2-5 cm down the tube and velocity became constant, images were taken for contact angle and velocity analysis. Capillary tubes were cleaned between runs and used multiple times throughout the experiment. The cleaning procedure can be found in the appendix.

3.4 Image analysis

Velocity and dynamic contact angle was determined using ImageJ (US National Institute of Mental Health), a Java based image processing program that supports image stacks. To account for the index of refraction, all velocity and radius measurements were adjusted by a factor of 0.93 following Hoffman [1975].

To measure the velocity, the position of the meniscus was measured on a series of subsequent images, noting the time that the image was recorded and the pixel position of the meniscus. The slug velocity was then calculated as Δpixels/Δtime and converted to m/s using the appropriate image resolution.

Two methods were used to determine the contact angles. For the protractor measurements [*Hoffman*, 1975], images of dynamic menisci were enlarged and lines were drawn on the liquid-solid-interface (XY), and the liquid-air interface (YZ) at the inflection point (Fig. 3a). The contact angle was then calculated by an ImageJ function. This was repeated for other side. Because the apparatus was not always perfectly level, left and right contact angles were measured and then averaged before further analyses. If left and right contact angles differed by more than 5° due to an unwanted tilting of the chamber causing a lack a symmetry, the data of run was not used.

For the apex-contact line method, the method utilized by Ngan and Dussan [1982, 1989] and simplified by Bian *et al.* [2003] was used. This method works well if one assumes that the interface contact line is the arc of a circle using:

$$\theta_{ave} = \pi/2 - 2\arctan(h/R) \quad (3)$$

where θ_{ave} is the average advancing contact angle; h is the distance (using consistent Cartesian coordinates) between the midpoint of A and B from C. R is the radius of the viewed capillary tube (Fig. 3b).

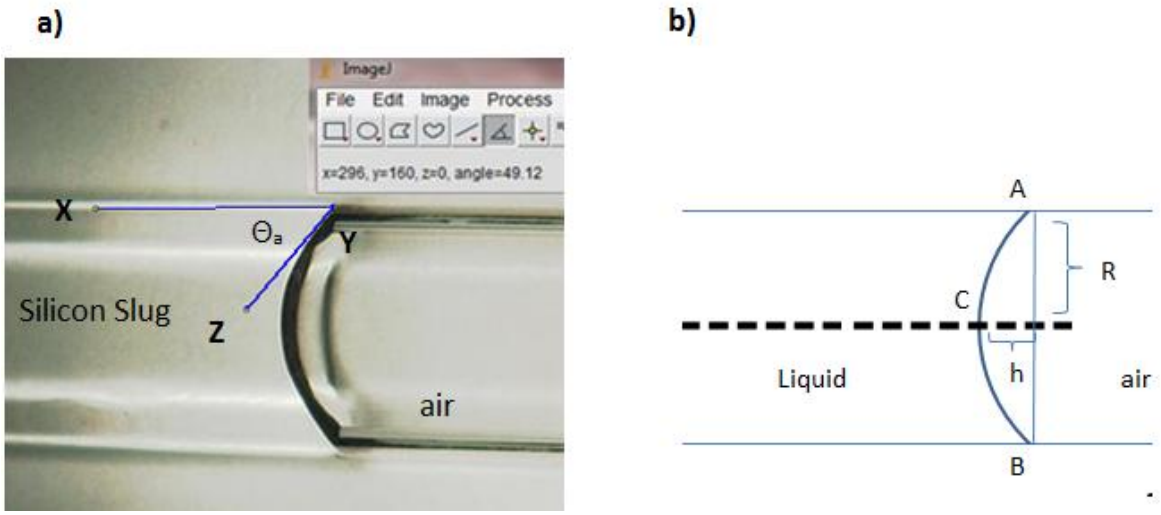

Figure 3a) Protractor method measurement of contact angle (θ_a) in a capillary, with lines drawn (XYZ) for calculation of the contact angle; and 3b) apex method of measuring contact angle that uses the Cartesian coordinate values of the point where the liquid, capillary tube and air meet (A, B) and the position where the liquid and air intersect at the radius of the capillary (C).

Table 2 Experimental design, showing the number of replicates (n) performed for the different combinations of liquid type (order based on increasing viscosity) and chamber size.

	Chamber size (width x depth, mm)*			
Liquid	**2 x 4**	**2 x 6**	**3.5 x 9**	**3.85 x 11.95**
V100	n=19	n=32	b	b
V500	a	n=39	n=19	b
Glycerin	n=24	n=34	n=31	b
V30000	a	n=26	n=38	n=19
V100000	a	a	n=43	n=10

* The letter "a" signifies where the fluid was too viscous to pipette into the chamber, and "b" signifies where the liquid was not viscous enough in the larger chamber and prone to sliding along one side of the chamber or the recording speed was not fast enough.

4. Results and Discussion

4.1 Relationship between Froude and Reynolds number

Three hundred and thirty four experimental runs were performed using 12 liquid/chamber size combinations, recording velocity and dynamic contact angle (Table 2). Fig. 4 plots the Froude against the Reynolds' number for 12 liquid/chamber size combinations.

$$\frac{Fr}{Re} = \frac{\frac{inertia}{gravity}}{\frac{inertia}{viscosity}} = \frac{viscosity}{gravity} = \frac{\mu v}{\rho g r^2} \quad (4)$$

The observed linear relationship shown in Figure 4 between Froude and Reynolds' number for the red square points indicate that Poiseuille's Law applies as the slugs were sufficiently long. This is the case when the flow at the tip and end of slug have negligible impact. The points in blue diamonds that deviate from the line were done with shorter slugs at low inclinations and show that Poiseuille's Law does not apply, meaning that end effects should not be used in the subsequent analysis.

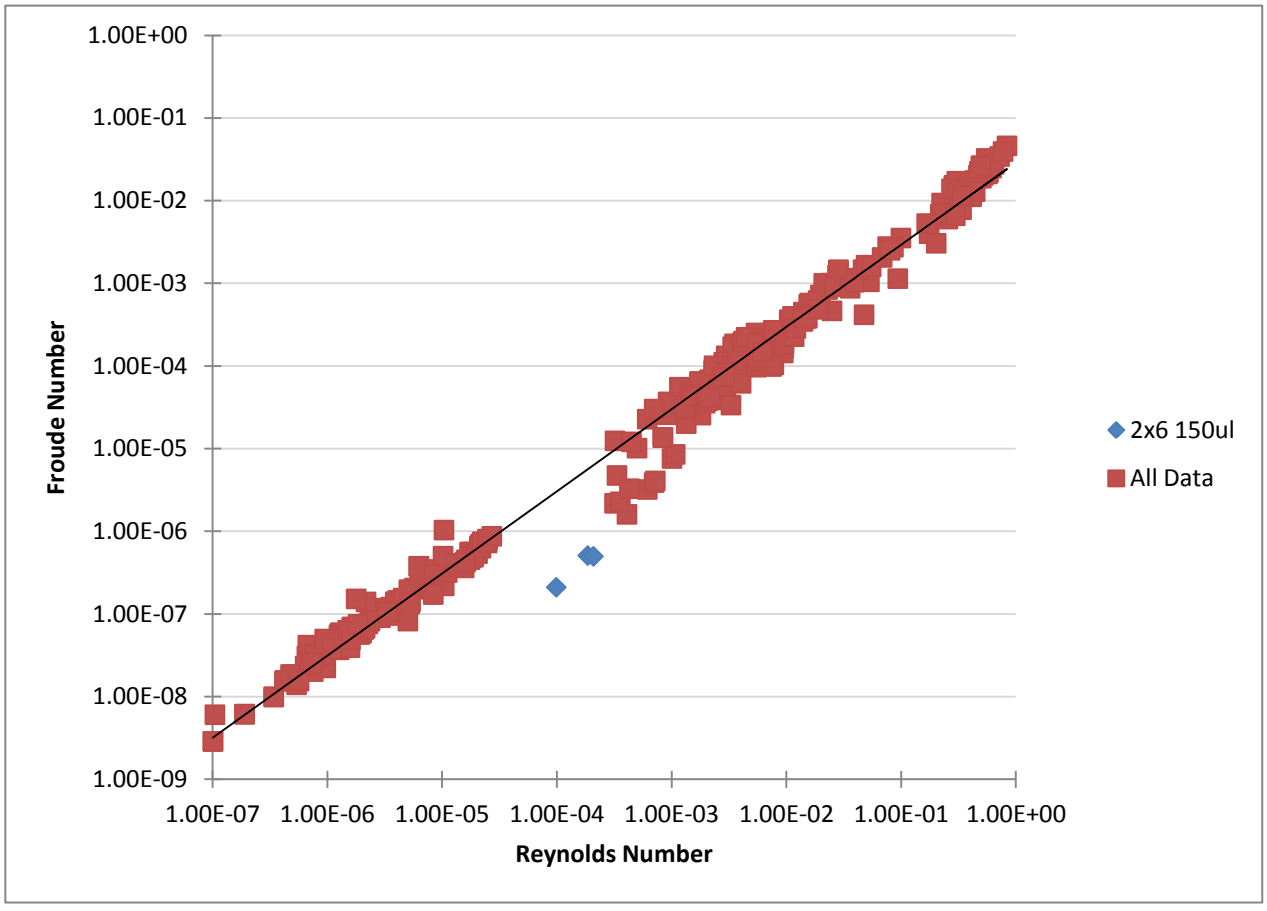

Figure 4: Froude vs. Reynolds Number (n=336 for 5 different liquids and 4 chamber sizes (Table A1), in which red squares indicate experimental results that followed Poiseuille's Law, and blue diamonds that did not. A linear regression line is fitted (R^2=0.9916).

Fig. 5a shows the measured dynamic contact angles plotted against their capillary number. Although there is considerable scatter between the various liquid/chamber size combinations, as wetting speed increases, dynamic contact angles increase as observed by Hoffman [1975]. Applying Hoffman's shift as described in section 2 to reduce scatter barely improved the R^2 value. Our $\theta_s = 0$ data is reduced to a best fit line (purple line) and applying Jiang's equation (2) on our using $\theta_s = 0°$ line with a θ_s of 34° (blue line) for glycerin also not predict our experimental data (green line) adequately in Fig 5b.

Therefore, we introduce a reduced contact angle (θ_r) defined as

$$\theta_r = \frac{\theta_m - \theta_s}{(180 - \theta_s)} * 180 \qquad (5)$$

Plotting the data this way improves the R^2 from 0.63 to 0.86. Comparison of Hoffman [1975] curve (thin black line in Fig. 5c) and our average curve (thick black line in Fig. 5c) shows they coincide at the high capillary numbers. At lower capillary numbers, our contact angles were slightly greater than Hoffman. Our average curve of the reduced data is also slightly greater than Jiang's equation.

From our data, $\theta_s=0$ is not a unique curve as our data obtained with liquids with $\theta_s=0$ does not match exactly the results of Hoffman, however this could possibly be due to the rectangular geometry instead of a cylindrical tubut used in Hoffman's experiments.

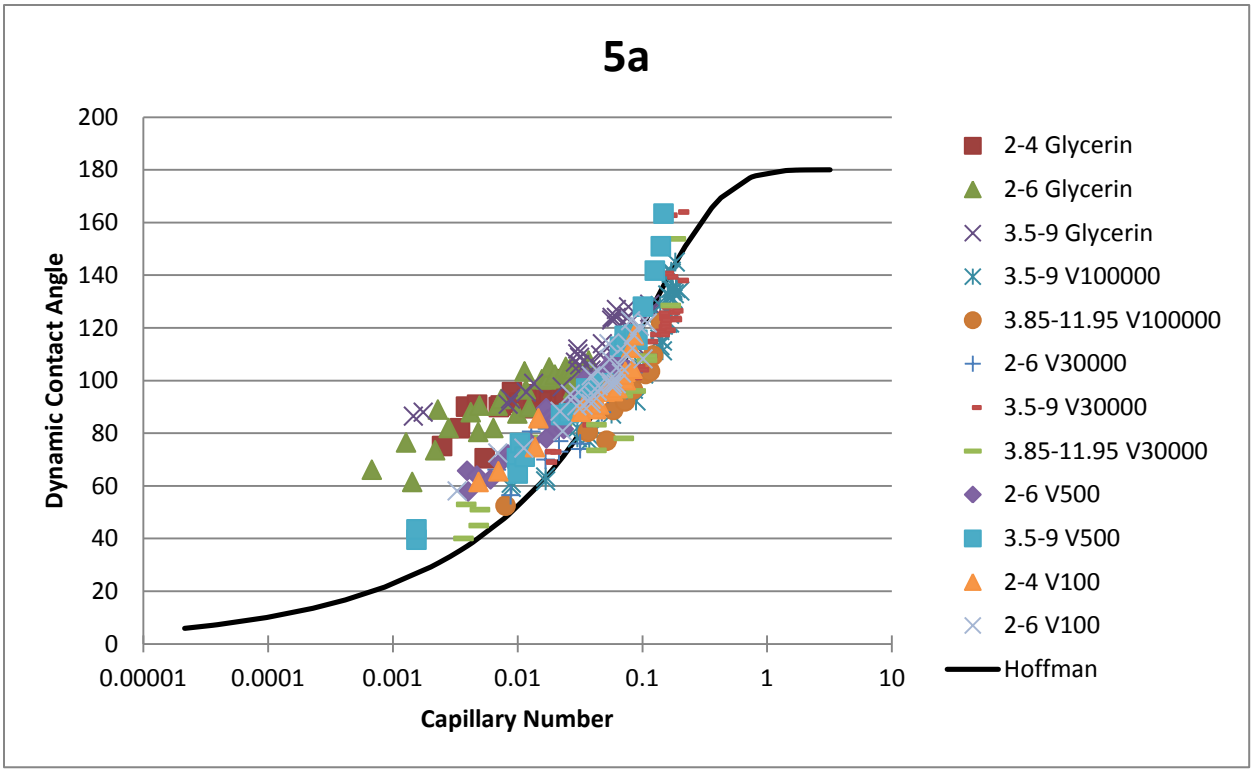
5a
Dynamic Contact Angle
200
180
160
140
120
100
80
60
40
20
0
0.00001
0.0001
0.001
0.01
0.1
1
10
Capillary Number
2-4 Glycerin
2-6 Glycerin
3.5-9 Glycerin
3.5-9 V100000
3.85-11.95 V100000
2-6 V30000
3.5-9 V30000
3.85-11.95 V30000
2-6 V500
3.5-9 V500
2-4 V100
2-6 V100
Hoffman

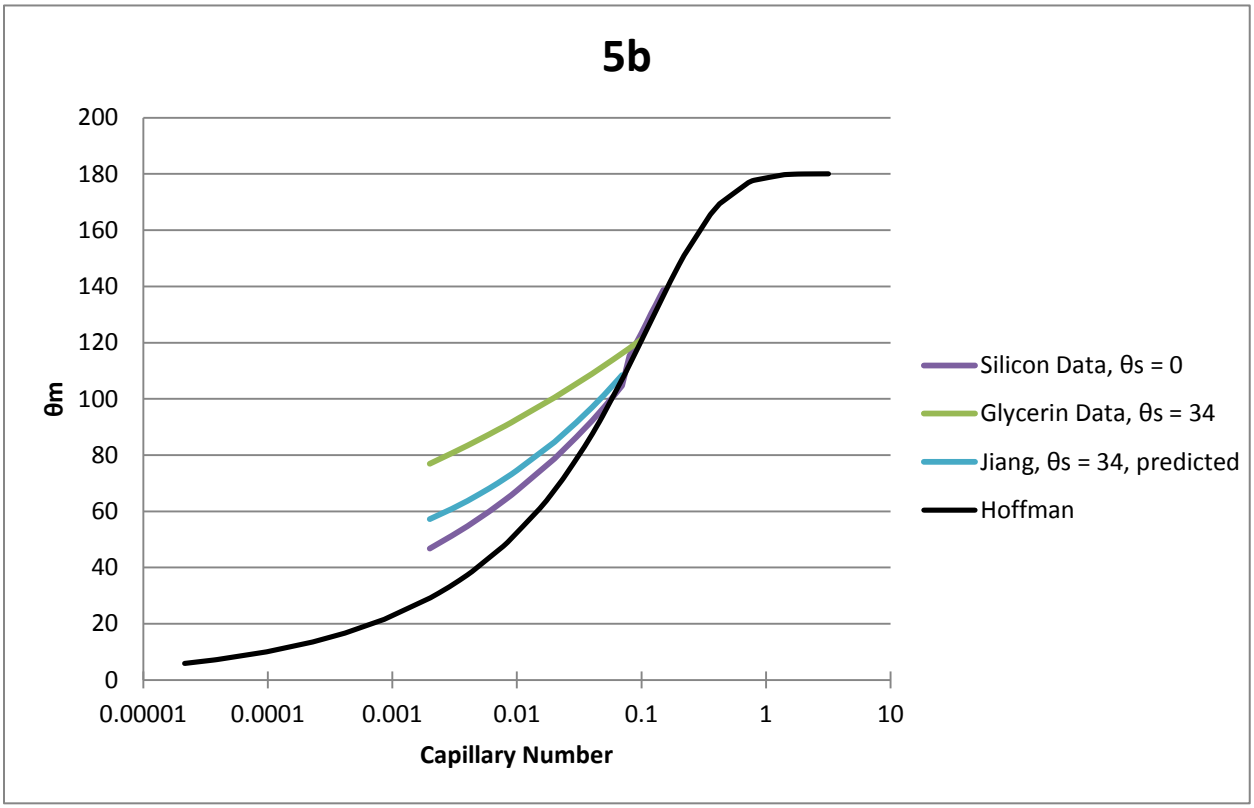
5b
θm
200
180
160
140
120
100
80
60
40
20
0
0.00001
0.0001
0.001
0.01
0.1
1
10
Capillary Number
Silicon Data, θs = 0
Glycerin Data, θs = 34
Jiang, θs = 34, predicted
Hoffman

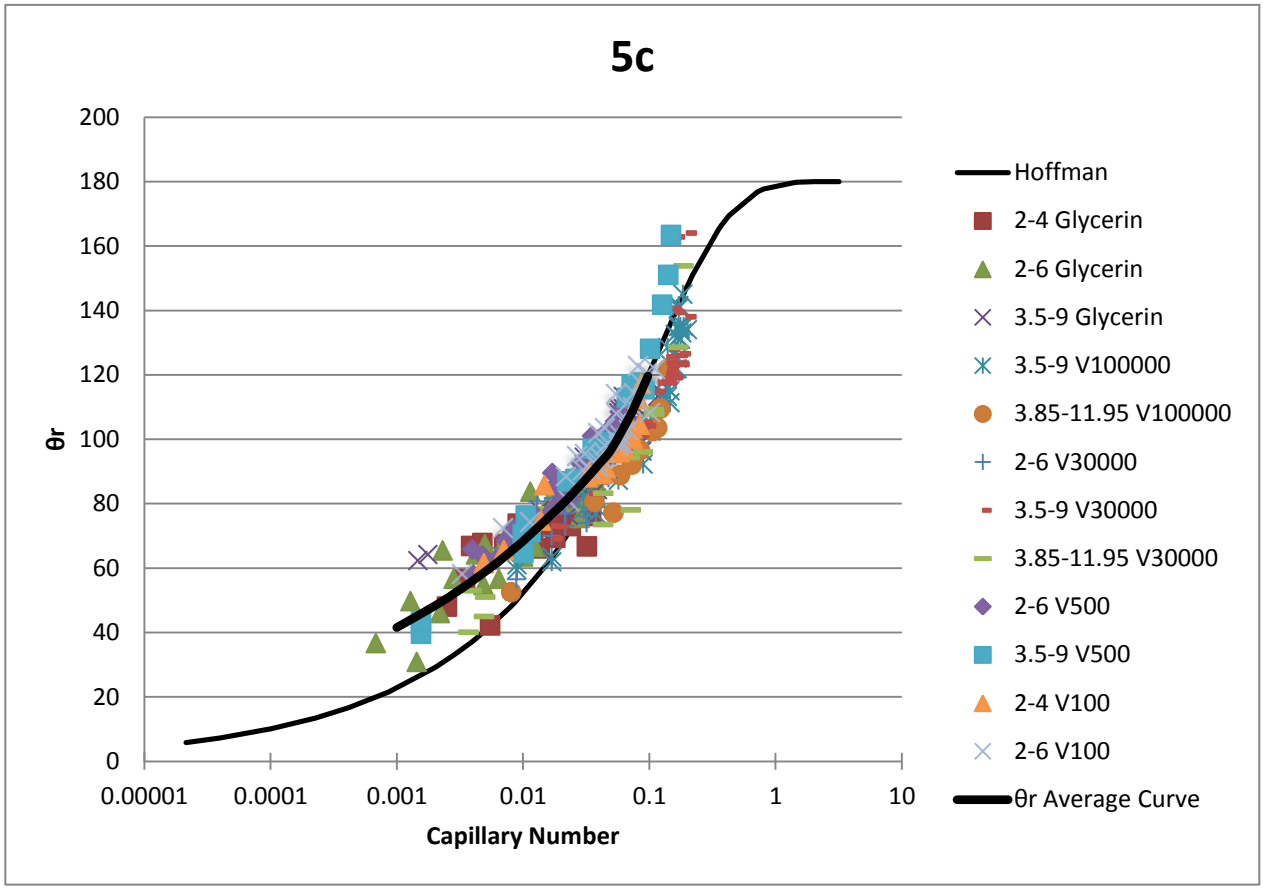

Figure 5: a) All experiment results plotted with dynamic contact angle as a function of capillary number with the results of Hoffman (1975), R^2 = 0.63, b) The best fit line for the glycerin data is plotted with our $\theta_s = 0°$ line from our experiment data and Jiang's correction(eqn. 2) based on our $\theta_s = 0°$ line using θ_s as 34° as a function of capillary number, c) All experiment results are plotted as a reduced dynamic contact angles; $\theta_{Reduced} = \frac{\theta_m - \theta_s}{(180 - \theta_s)} * 180$ as a function of capillary number; R^2=0.86 with an average curve.

4.2 Size Effects and importance of correct analysis of interface shape

Some researchers [*Ngan and Dussan V.*, 1982; 1989; *Legait and Sourieau*, 1985] propose that with larger size, dynamic contact angle increases. In our experiments with 2x4 mm and 2x6 mm chambers, non-circular interfaces were not observed. However, larger capillary tubes (3.5 x 9 mm, 3.85-11.95 mm) were prone to asymmetric contact lines and non-circular interfaces (Table E1).

The protractor method and apex method were used to measure dynamic contact angles. For angles between 60°-120° within 2x4, 2x6 mm tubes, we found that the interface was consistently circular and the protractor method was a sufficient way for measuring contact angle in this range as long as the contact line was nearly symmetrical. For the data outside this range within the 2x4 and 2x6 mm tubes, the apex method was used after verifying the contact line was circular because Ngan and Dussan [1982] point out that the protractor method is subjective. As the capillary size increased, a comparison between the two methods showed that the apex-contact line method overestimated the dynamic contact angle due to the frequency of non-circular interfaces (Figure 6). Because contact angle measurement with the protractor method is less consistent for angles <60° or >120°, the apex-contact line method was used for data in this range. Data was included with the apex method up to 165° but data above 140° was not used for analysis due to overestimation from apex method.

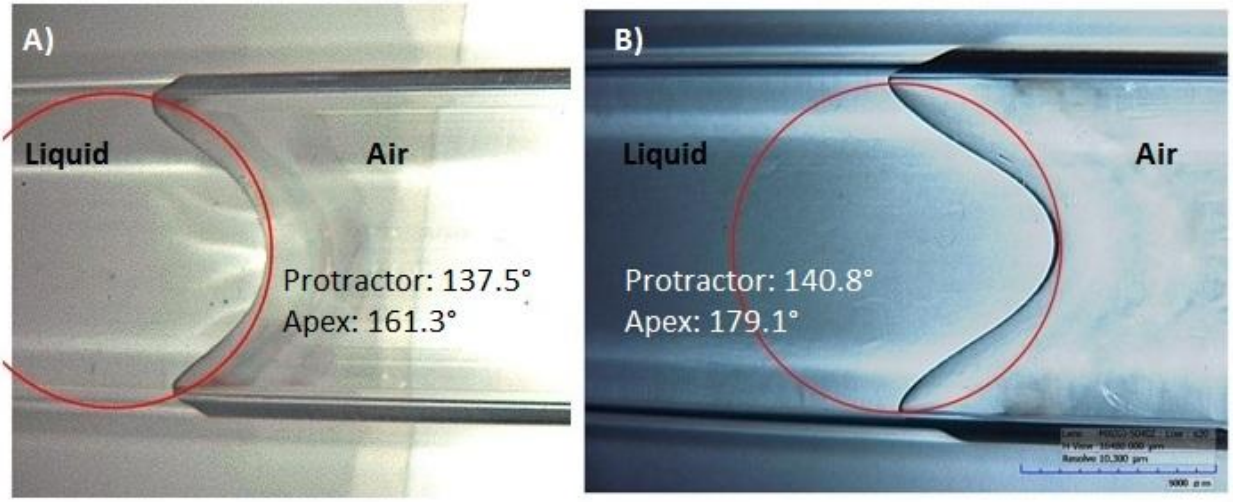

Figure 6: Comparison of aped-contact line method and protractor method on non-circular interfaces. Image A is a 3.5-9 mm chamber, image B is 3.85-11.95 mm chamber.

The question remains how dynamic contact angles relate to instability in soil. It is immediately clear that for fluxes in soil during natural infiltration of 0.1-10 cm/h (related capillary numbers of 2×10^{-7} to 2×10^{-5}) the dynamic contact angle is hardly different from the static contact angle. However we assume that the pressure at the wetting front has to build up before it is large enough so that the water can go through the pore neck. Immediately after the water is released, the pressure drops and then build up again until the water breaks though in the following pore. We have seen this phenomenon during imbibition from the bottom (with much lower velocities than wetting fronts) where one pore "pops" at a time. Thus in the experiment of Glass *et al*. [1989] for a typical 1.5 cm wide finger in a 1 cm wide chamber, the flux in the finger is approximately 10 cm^3/min and assuming that this flux has to go through a neck with a radius of 0.21 mm results in a velocity in the pore neck of approximately 1.2 m/sec with capillary number of 0.015 and a dynamic contact angle of 60 degrees according to the Hoffman curve. This 60 degree angle then explains that the water still infiltrates in the soil but according to Laplace's equation at less negative pressure than a regular wetting front explaining the overshoot observed in DiCarlo's [2007] experiments. Thus by assuming that the imposed flux goes through the pore necks one at a time the dynamic contact angles seem to provide a general mechanism for instabilities in soils.

5. Conclusions

In conclusion, using rectangular capillaries allows us to view the interfaces without distortion, however the geometry may be responsible for the slight differences at $\theta_s=0$ with Hoffman's [1975] results. We found that by using a reduced dynamic contact angle, simplifies the analysis of the data. Size had no obvious impact on dynamic contact angles but we found constant circular interfaces in smaller diameter chambers and as the capillary size increases, the

interfaces begins to deviate from a circular meniscus. If we assumed that the interface was circular, it would lead to incorrectly large contact angles measurements when the apex method was used (Fig 6). And finally, dynamic contact angles can explain the overshoot observed or wet tip observed in finger experiments.

APPENDIX A

CLEANING PROCEDURE OF CAPILLARY TUBES

Capillary tubes coated with glycerin (which is water-soluble) were repeatedly flushed with high velocity DI water, and then dried with ethyl alcohol and pressurized air. The procedure was repeated until microscope showed no residue on the glass. Glassware coated with silicon was cleaned using a heated solution of sodium hydroxide pellets in a 95% solution of ethyl alcohol following Lowry [1997]. The cleaning procedure was repeated until no residue was present when the glass tube is examined with the microscope. In general, low viscosity silicon fluids were removed by leaving the capillary tubes in the ethyl alcohol and sodium hydroxide cleaning solution for 10 min, while overnight soaking of the tubes was required to clean out the more viscous silicon fluids.

APPENDIX B

ADDITIONAL DIMENSIONLESS NUMBERS

Other relevant dimensionless numbers to help understand slug flow include the Froude Number, Reynolds Number, Weber Number and Bond Number. The Froude Number is the ratio of inertia to gravity and is equal to

$$Fr = v^2 / g*r \quad (6)$$

where v is velocity (m/s), and g is gravity (m/s^2) and r is radius (m).

The Reynolds number is a ratio of between inertia and viscosity and used to classify a flow to be laminar or turbulent. Viscous flow dominates at low Reynolds number and inertial forces dominate at high Reynolds numbers. The Reynolds number is written as

$$Re = \rho v l / \mu \quad (7)$$

where ρ is fluid density (kg/m^3), v is the velocity (m/s) and l is characteristic length, diameter (m) and μ is the viscosity (Pa•s). In our experimental results, the Reynolds number for all of the data is less than 1, indicating all slug flows were laminar.

The Weber number relates inertia with surface tension and is written as

$$We = \rho v^2 l / \gamma \quad (8)$$

where ρ is the density of the fluid (g/ml), v is its velocity (m/s), l is its characteristic length (m) and γ is the surface tension (N/m).

The Bond number compares gravity to surface tension is written as:

$$Bo = \Delta\rho g\, r^2 / \gamma \quad (9)$$

where $\Delta\rho$ is density or density difference of the two phases, (kg/m^3), g is gravitational acceleration, (m/s^2), r is characteristic length, radius of capillary tube, (m) and γ is surface tension, (N/m). A high bond number indicates that surface tension does not play a strong role; a low bond number indicates that surface tension dominates.

APPENDIX C

STATIC CONTACT ANGLE OF GLYCERIN

The static contact angle has been measured to be about 30 degrees when measured inside of pyrex glass tube [*Bajpai and Khandekar*, 2012]. It has also been measured at 27±1° using a goniometer [*Senn*, 2007]. Other sources have a static contact angle around 70° [*Fermigier and Jenffer*, 1991; *Blake*, 2006] so that experimental data agreed with the theoretical results.

APPENDIX D

BRIEF MATHEMATICAL RELATIONSHIPS BACKGROUND

D.1 Introduction

One of the most frequent issues that come up with trying to predict the relationship between fluid properties and dynamic contact angles is the mathematical approach [*Blake*, 2006]. From fluid mechanics, the horizontal component of a Newtonian fluid increase as it approaches the wall of the solid. At the wall, this horizontal component (shear stress) of the fluid approaches an infinite value and consequently, this force should prevent the liquid from moving. We know this is not true from observation. This conundrum is referred to as a no-slip boundary condition. There are several main approaches to resolve this issue [*Blake,* 2006].

Frequently, the no-slip boundary condition is replaced with a slip boundary condition, i.e. relaxing the boundary condition at the solid liquid interface to allow for liquid adjacent to the wall to move [*Huh and Scriven*, 1971; *Thompson and Robbins*, 1989]. Another way to get around this issue is to use a precursor film; it has been observed that on a microscopic level, there is a microscopic liquid film moving ahead, forming a microscopic contact angle influenced by molecular diffusive properties ahead of the measured macroscopic contact angle [*Nieminen et al.*, 1992; *Burlatsky et al.*, 1996]. A more detailed description to the variety of approaches toward removing the singularity can be found in the work of other researchers [*Huh and Scriven*, 1971; *Dussan V. and Davis*, 1974; *Dussan*, 1979; *de Gennes*, 1985; *Blake*, 2006].

Two main theories provide simple analytical equations using simplified physics for relating the dynamic contact angle to the wetting velocity: Hydrodynamic Theory (HDT) and Molecular Kinetic Theory (MKT). These two approaches relate dynamic contact angle with

velocity through measureable parameters however they differ with their approach to friction [*Brochard-Wyart and De Gennes*, 1992; *Blake*, 2006; *Ralston et al.*, 2008]. For brevity, we will only cover the necessary points, as a full description the mathematical approach is beyond the scope of this thesis but more details on these approaches can be found in the work of Blake [2006] and Ralston *et al.* [2008].

D.2 Hydrodynamic Theory

First, hydrodynamic theory [*Huh and Scriven*, 1971; *Voinov*, 1977; *Dussan*, 1979; *de Gennes*, 1985; *Cox*, 1986] assumes the viscous dissipation occuring within the wedge of liquid between the precursor film and transition zone is the main source of friction. The viscous bending occurs at the liquid/vapor interface occurs in the mesoscopic region and can be observed through the macroscopic (experimentally observed) contact angle [*Blake*, 2006]. The hydrodynamic theory can be expressed with the following equation:

$$\theta_D^3 - \theta_m^3 \approx 9 * Ca \ln\left(\frac{L}{L_m}\right) \quad (10)$$

where θ_D is the dynamic contact angle; θ_m is the local microscopic angle (usually considered static contact angle), refer to Voinov [1977]; L and Lm are chosen macroscopic and microscopic length scales, respectively, where continuum theories fail. Frequently, it is highlighted by other researchers that the main weakness of the HDT is that it does not specifically consider the contribution of surface properties such as solid roughness and geometry that would contribute to frictional processes occurring between the liquid and solid [*Dussan V.*, 1976; *Blake*, 2006].

D.3 Molecular Kinetic Theory

Second, in the molecular kinetic theory [*Blake and Haynes*, 1969] friction resistance is assumed to consist of mainly of dissipation, which is related to the hopping frequency of molecules between sorption sites and contact line at the molecular edge of the liquid film. Put another way, molecular kinetic theory is based on the disturbance of adsorption equilibria and surface tension at the wetting line [*Blake and Haynes*, 1969; *Cherry and Holmes*, 1969; *Blake*, 2006]. The main equation for the MKT applicable to the results in this paper is below.

$$U = 2k^0\lambda\sinh[\gamma(\cos\theta_s - \cos\theta_D)\lambda^2/2k_BT] \quad (11)$$

where U is the velocity (m/s); k^0 is the equilibrium frequency of the random molecular displacements occurring within three phase zone; λ is equal to the average distance of each displacement; γ is the surface tension of the liquid (N/m); θ_D is the dynamic contact angle; θ_S is the static contact angle; k_B is equal to the Boltzmann's constant and T is the temperature (°K). The relationship incorporates both measurable quantities and microscopic properties. The $\gamma(\cos\theta_s-\cos\theta_D)$ comes from the theory that the driving force is the out of balance tension force [*Blake and Haynes*, 1969]. It is important to note that λ and k^o are not clearly developed and values cannot be consistently predicted [*Blake*, 2006]. Statistical techniques are needed to determine the best values for best curve fitting. These are two analytical approaches that are easy to apply, however as observed by Blake [2006] neither of these approaches is satisfactory for all situations.

D.4 Results

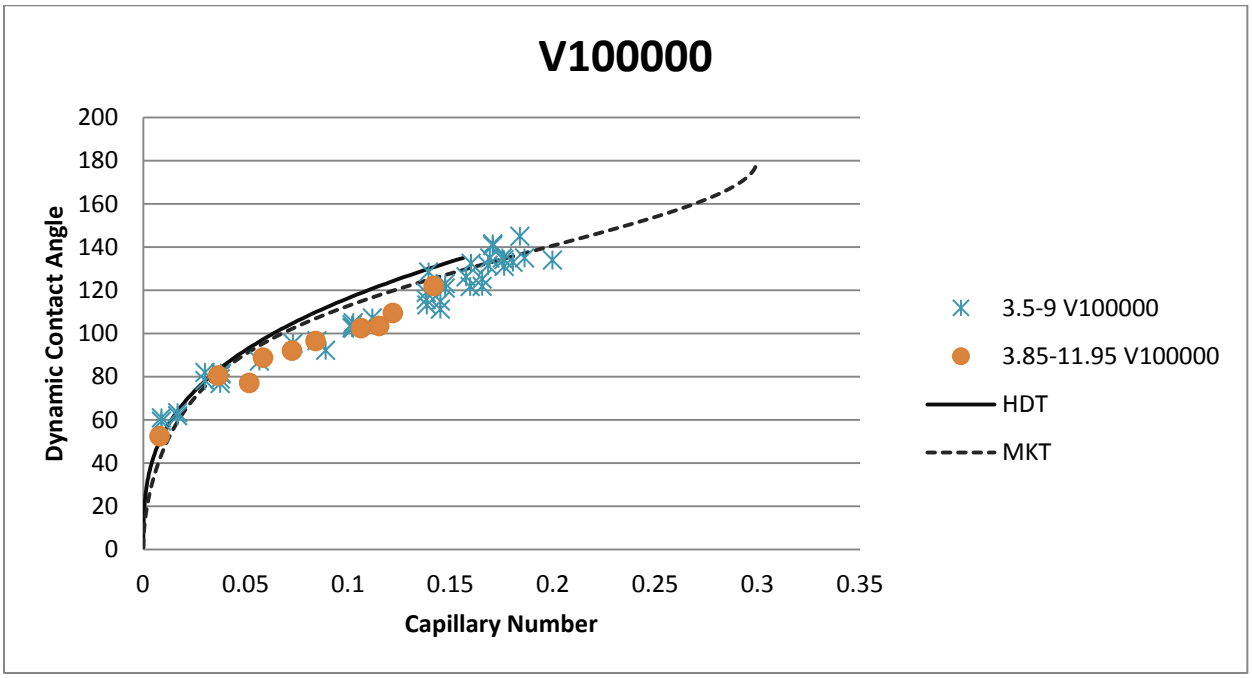

Figure D1: Dynamic contact angle of V100000 silicon oil on rectangular capillary tube. Solid curve: Hydrodynamic theory, eq (10), ln(L/Lm) = 9.3. Dashed curve: MKT, eq (11), λ = .80 nm, and k^0 = 2300 and θ_s = 0 in both cases.

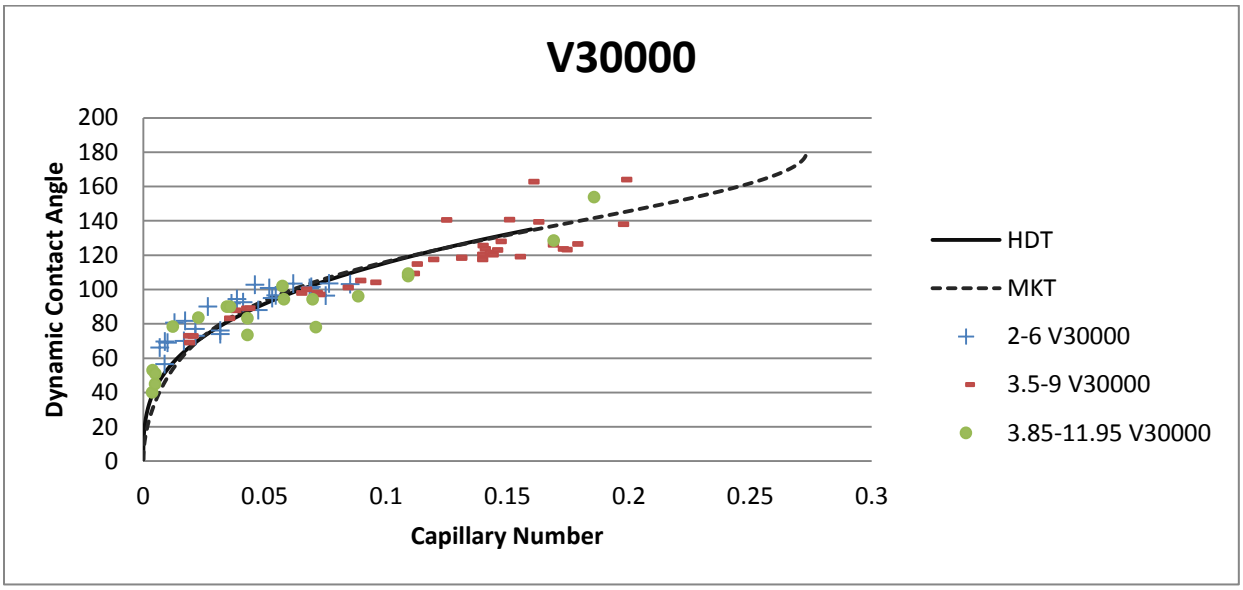

Figure D2: Dynamic contact angle of V30000 silicon oil on rectangular capillary tube. Solid curve: Hydrodynamic theory, eq (10), ln(L/Lm) = 9.1. Dashed curve: MKT, eq (11), λ = .80 nm, and k^0 = 7000 and θ_s = 0 in both cases.

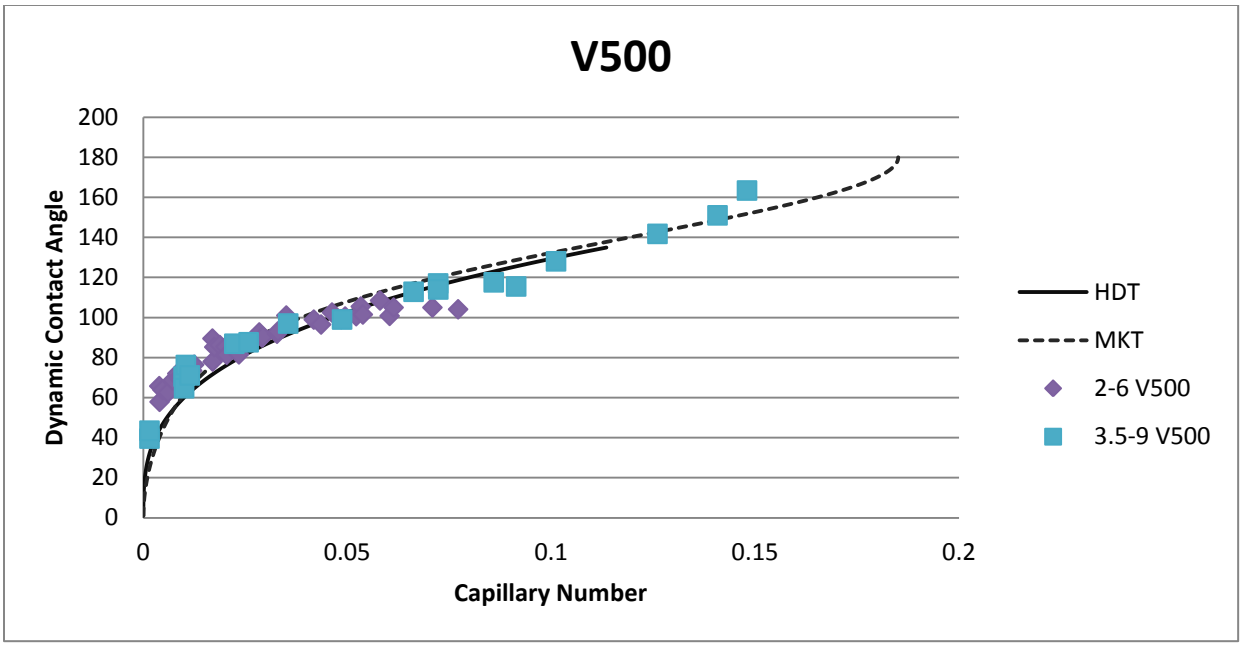

Figure D3: Dynamic contact angle of V500 silicon oil on rectangular capillary tube. Solid curve: Hydrodynamic theory, eq (10), ln(L/Lm) = 12.8. Dashed curve: MKT, eq (11), λ = .80 nm, and k^0 = 221098 and $\theta_s = 0$

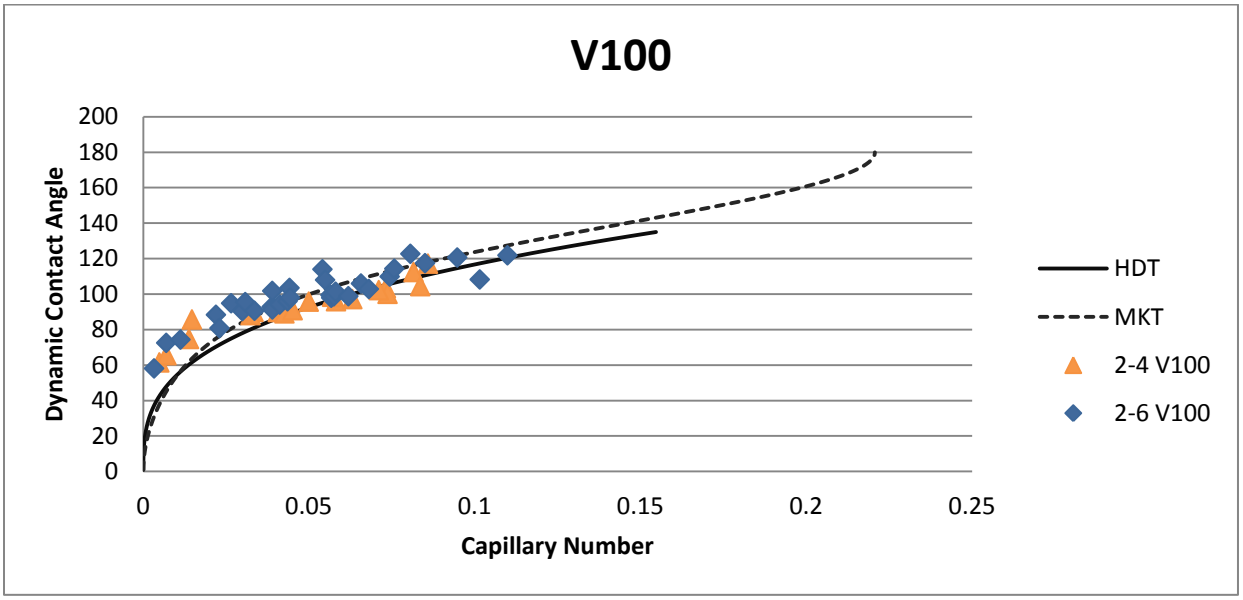

Figure D4: Dynamic contact angle of V100 silicon oil on rectangular capillary tube. Solid curve: Hydrodynamic theory, eq (10), ln(L/Lm) = 9.4. Dashed curve: MKT, eq (11), λ = .80 nm, and k^0 = 185000 and $\theta_s = 0$ in both cases.

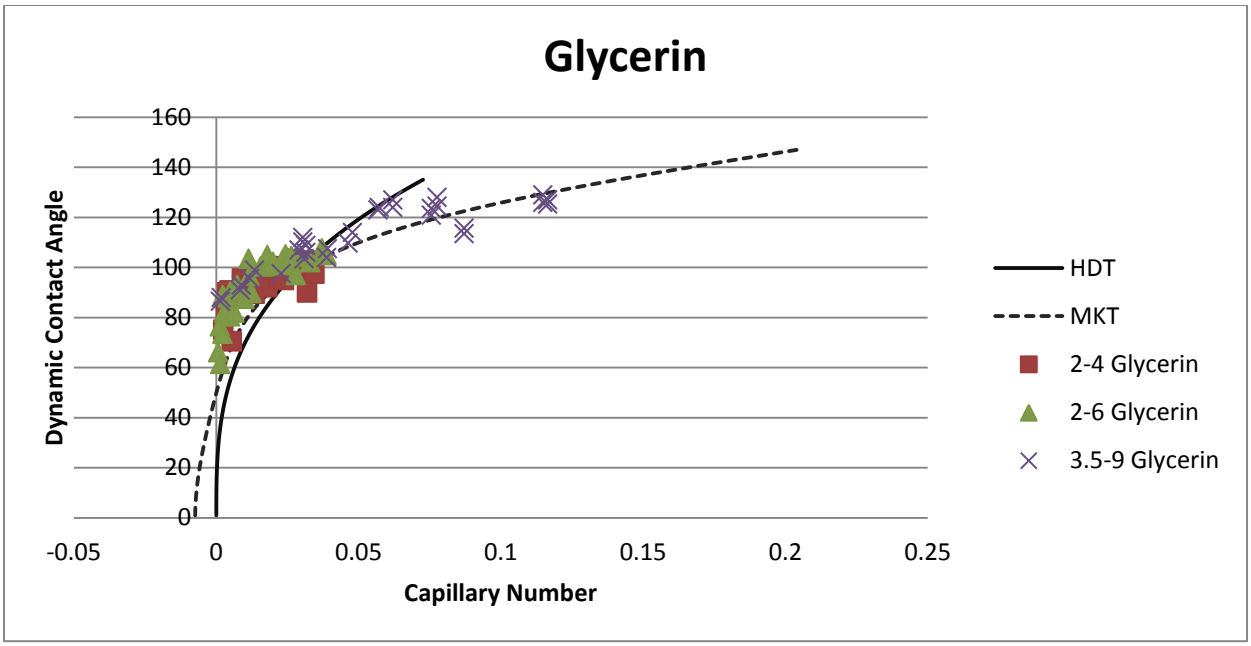

Figure D5: Dynamic contact angle of glycerin on rectangular capillary tube. Solid curve: Hydrodynamic theory, eq (10), ln(L/Lm) = 20 and θ_s= 50. Dashed curve: MKT, eq (11), $\lambda = 6*10^{-10}$ nm, and k^0 = 250000 and θ_s = 50.

D.5 Discussion and Conclusions

By observation, we can see that both HDT and MKT both match our experiment data reasonably well. The HDT equation (eqn. 10) was truncated at 135° as done by Voinov [1977]. Our λ value was taken from Blake [2006]. L and L_m values (eqn. 10) and k^o values (eqn. 11) were in the same order as Blake. The MKT matched our glycerin experimental data slightly better than the HDT approach as observed by Blake [2006]. However, for the glycerin data, the θ_s was used as a fitting parameter and using θ_s = 34° as experimentally measured resulted in a poor fit between HDT and MKT equations and our experimental data. As found by other researchers, HDT and MKT both match completely wetting liquids (silicon) better than non-completely wetting liquids. This leads to the common conclusion that neither approach is fully robust and that it is likely both sources of friction from MKT and HDT approach play a role in dynamic wetting [*Blake*, 2006].

APPENDIX E

ADDITIONAL TABLES AND GRAPHS OF EXPERIMENTAL DATA

Table E1: Replicates In the case of V100000 and V30000 fluid, the meniscus began to deviate from a circular shape and approached a parabolic profile at high inclinations indicated with an X.

inclination	Glycerin			V100		V500		V30000			V100000	
(°)	A*	B	C	A	B	B	C	B	C	D	C	D
1	0	0	0	0	0	0	2	0	0	5	0	1
2.5	0	0	0	0	0	0	0	0	1	0	0	0
3	0	0	0	0	0	0	0	0	0	0	2	0
5	1	0	2	1	1	4	4	3	2	4	2	0
6	0	0	0	0	0	0	0	0	0	0	0	1
6.8	0	0	0	0	0	0	0	0	0	0	0	1
10	3	2	3	0	2	4	2	3	3	3	6	2
15	3	0	1	1	0	2	2	3	1	1	1	1
20	1	3	2	0	1	4	0	3	3	2	2	2
25	0	0	0	0	0	1	0	0	1	0	1	1
30	2	6	4	5	6	5	5	2	2	2	4	1
35	0	0	0	0	0	0	0	1	0	0	2	X
40	1	1	0	1	1	1	1	1	3	0	1	X
45	4	7	2	1	5	4	1	2	4	2	4	X
50	1	1	2	0	0	2	1	1	4	X	1	X
55	0	0	0	0	0	0	0	0	0	X	3	X
60	1	6	6	5	6	5	1	3	8	X	2	X
65	0	0	2	0	0	0	0	0	0	X	0	X
70	5	3	3	2	1	2	0	1	2	X	5	X
75	0	0	2	0	0	0	0	0	0	X	3	X
80	2	4	2	3	9	4	0	3	1	X	3	X
85	0	0	0	0	0	1	0	0	3	X	1	X
90	0	1	0	0	0	0	0	0	0	X	0	X

*A = 2x4 mm, B = 2x6 mm, C = 3.5x9 mm, D = 3.85-11.95 mm

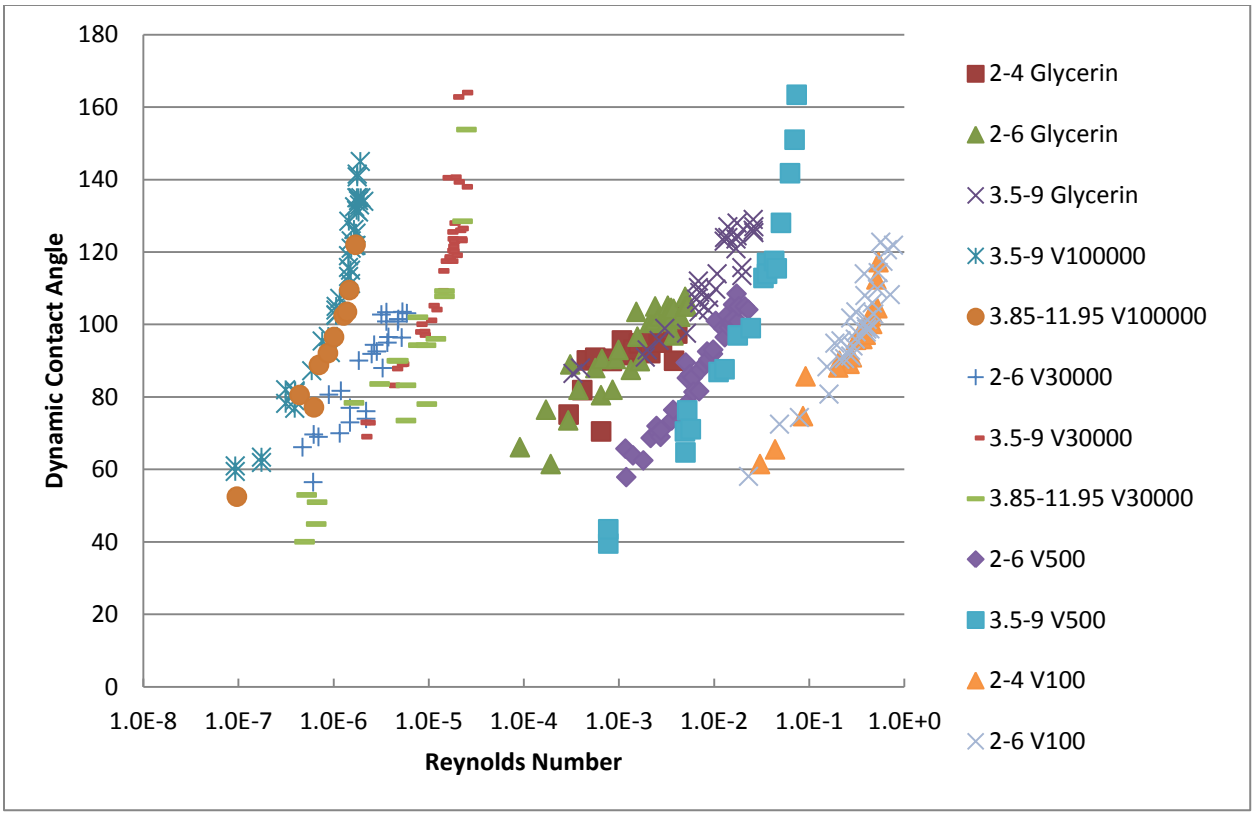

Figure E1: Experimental Results plotted as a function of Reynolds number.

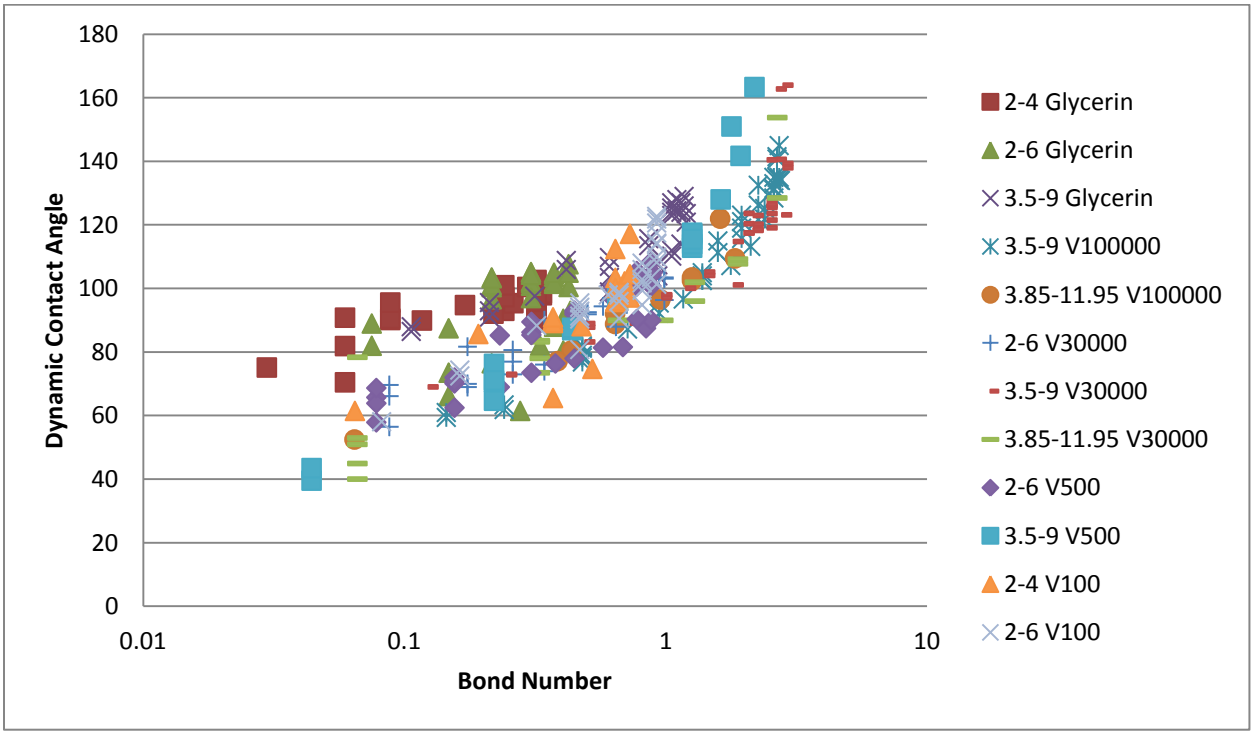

Figure E2: Experimental Results plotted as a function of Bond Number.

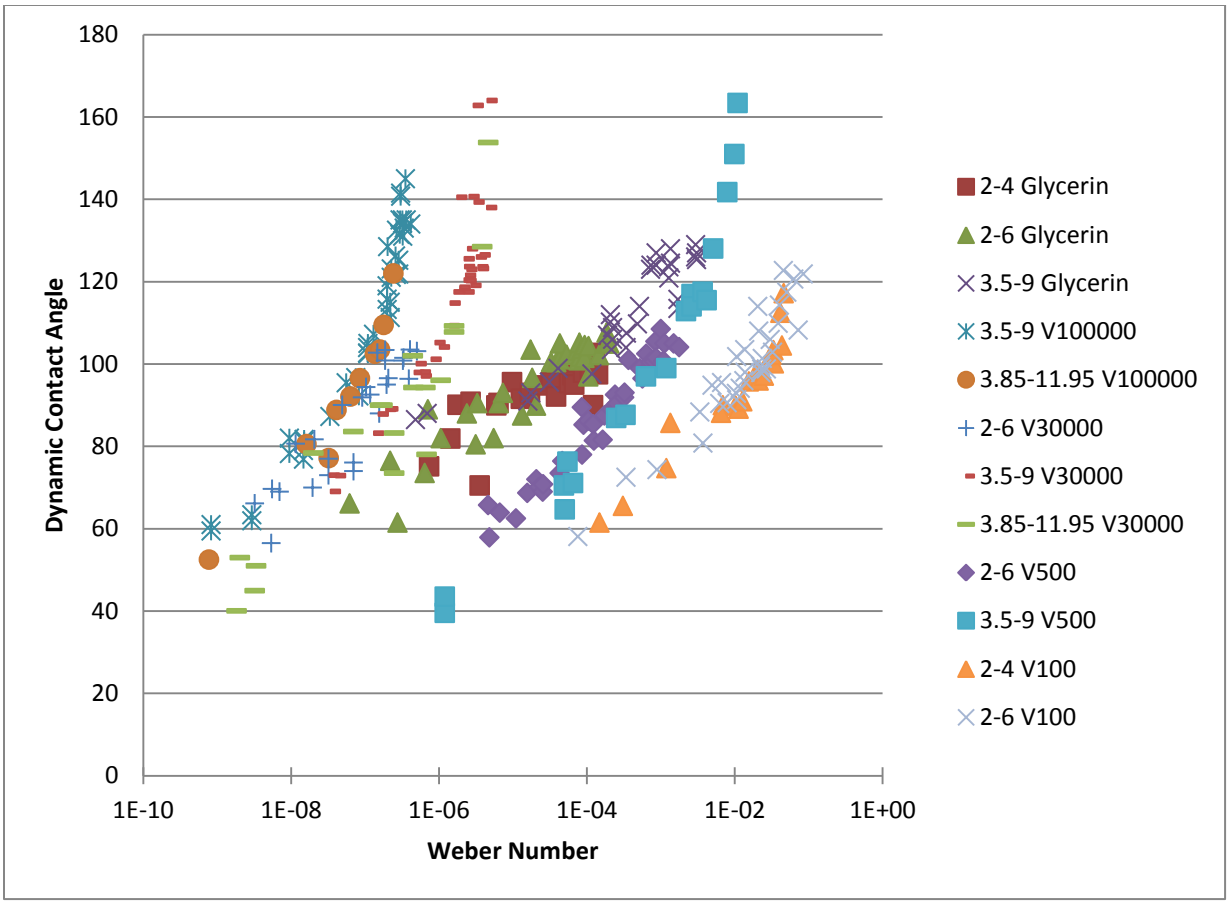

Figure E3: Experimental Results plotted as a function of Weber Number.

.

Table E2: All experiment data

Chamber (mm * mm)	Radius d (m)	Radius D (m)	Radius (m)	Liquid (name)	Density (kg/m^3)	Tilt (degree)	Velocity (m/s)	Velocity ADJUSTED	Viscosity (Pa.s)	S Tension (N/m)	DCA used	Ca ($\mu v/\gamma$)
2-4	0.002	0.004	0.0013	Gly	1253.6	5	1.28E-04	1.19E-04	1.340	0.064	75.15	0.0025
2-4	0.002	0.004	0.0013	Gly	1253.6	10	1.79E-04	1.65E-04	1.340	0.064	81.90	0.0035
2-4	0.002	0.004	0.0013	Gly	1253.6	15	2.00E-04	1.85E-04	1.340	0.064	90.10	0.0039
2-4	0.002	0.004	0.0013	Gly	1253.6	10	2.45E-04	2.27E-04	1.340	0.064	90.84	0.0047
2-4	0.002	0.004	0.0013	Gly	1253.6	10	2.82E-04	2.61E-04	1.340	0.064	70.50	0.0055
2-4	0.002	0.004	0.0013	Gly	1253.6	20	3.66E-04	3.38E-04	1.340	0.064	89.95	0.0071
2-4	0.002	0.004	0.0013	Gly	1253.6	15	3.78E-04	3.50E-04	1.340	0.064	90.55	0.0073
2-4	0.002	0.004	0.0013	Gly	1253.6	15	4.67E-04	4.32E-04	1.340	0.064	95.60	0.0090
2-4	0.002	0.004	0.0013	Gly	1253.6	70	5.36E-04	4.96E-04	1.340	0.064	91.55	0.0104
2-4	0.002	0.004	0.0013	Gly	1253.6	45	6.17E-04	5.71E-04	1.340	0.064	92.99	0.0120
2-4	0.002	0.004	0.0013	Gly	1253.6	30	6.98E-04	6.46E-04	1.340	0.064	89.50	0.0135
2-4	0.002	0.004	0.0013	Gly	1253.6	30	7.04E-04	6.51E-04	1.340	0.064	94.80	0.0136
2-4	0.002	0.004	0.0013	Gly	1253.6	45	8.56E-04	7.92E-04	1.340	0.064	95.65	0.0166
2-4	0.002	0.004	0.0013	Gly	1253.6	40	9.27E-04	8.57E-04	1.340	0.064	92.10	0.0180
2-4	0.002	0.004	0.0013	Gly	1253.6	50	1.14E-03	1.05E-03	1.340	0.064	95.40	0.0220
2-4	0.002	0.004	0.0013	Gly	1253.6	45	1.19E-03	1.11E-03	1.340	0.064	97.33	0.0231
2-4	0.002	0.004	0.0013	Gly	1253.6	60	1.22E-03	1.13E-03	1.340	0.064	100.50	0.0237
2-4	0.002	0.004	0.0013	Gly	1253.6	70	1.23E-03	1.14E-03	1.340	0.064	95.00	0.0238
2-4	0.002	0.004	0.0013	Gly	1253.6	45	1.41E-03	1.31E-03	1.340	0.064	101.05	0.0274
2-4	0.002	0.004	0.0013	Gly	1253.6	80	1.42E-03	1.31E-03	1.340	0.064	97.90	0.0274
2-4	0.002	0.004	0.0013	Gly	1253.6	80	1.57E-03	1.45E-03	1.340	0.064	98.50	0.0304
2-4	0.002	0.004	0.0013	Gly	1253.6	70	1.65E-03	1.53E-03	1.340	0.064	90.00	0.0319
2-4	0.002	0.004	0.0013	Gly	1253.6	70	1.69E-03	1.56E-03	1.340	0.064	102.70	0.0327
2-4	0.002	0.004	0.0013	Gly	1253.6	70	1.78E-03	1.65E-03	1.340	0.064	97.50	0.0345
2-6	0.002	0.006	0.0015	Gly	1253.6	20	3.51E-05	3.25E-05	1.340	0.064	66.15	0.0007
2-6	0.002	0.006	0.0015	Gly	1253.6	30	6.60E-05	6.11E-05	1.340	0.064	76.50	0.0013
2-6	0.002	0.006	0.0015	Gly	1253.6	40	7.40E-05	6.85E-05	1.340	0.064	61.50	0.0014

Table E2 (Continued)

Chamber (mm * mm)	Radius d (m)	Radius D (m)	Radius (m)	Liquid (name)	Density (kg/m^3)	Tilt (degree)	Velocity (m/s)	Velocity ADJUSTED	Viscosity (Pa.s)	S Tension (N/m)	DCA used	Ca ($\mu v/\gamma$)
2-6	0.002	0.006	0.0015	Gly	1253.6	20	1.13E-04	1.05E-04	1.340	0.064	73.55	0.0022
2-6	0.002	0.006	0.0015	Gly	1253.6	10	1.19E-04	1.10E-04	1.340	0.064	89.00	0.0023
2-6	0.002	0.006	0.0015	Gly	1253.6	50	1.45E-04	1.34E-04	1.340	0.064	82.00	0.0028
2-6	0.002	0.006	0.0015	Gly	1253.6	60	2.18E-04	2.02E-04	1.340	0.064	88.00	0.0042
2-6	0.002	0.006	0.0015	Gly	1253.6	70	2.50E-04	2.31E-04	1.340	0.064	80.50	0.0048
2-6	0.002	0.006	0.0015	Gly	1253.6	70	2.56E-04	2.37E-04	1.340	0.064	90.50	0.0050
2-6	0.002	0.006	0.0015	Gly	1253.6	10	3.31E-04	3.06E-04	1.340	0.064	82.00	0.0064
2-6	0.002	0.006	0.0015	Gly	1253.6	80	3.58E-04	3.31E-04	1.340	0.064	90.50	0.0069
2-6	0.002	0.006	0.0015	Gly	1253.6	90	3.82E-04	3.53E-04	1.340	0.064	93.00	0.0074
2-6	0.002	0.006	0.0015	Gly	1253.6	20	5.15E-04	4.76E-04	1.340	0.064	87.50	0.0100
2-6	0.002	0.006	0.0015	Gly	1253.6	30	5.88E-04	5.44E-04	1.340	0.064	103.50	0.0114
2-6	0.002	0.006	0.0015	Gly	1253.6	30	6.03E-04	5.58E-04	1.340	0.064	96.65	0.0117
2-6	0.002	0.006	0.0015	Gly	1253.6	70	6.40E-04	5.92E-04	1.340	0.064	89.90	0.0124
2-6	0.002	0.006	0.0015	Gly	1253.6	80	8.09E-04	7.48E-04	1.340	0.064	100.50	0.0157
2-6	0.002	0.006	0.0015	Gly	1253.6	30	8.77E-04	8.11E-04	1.340	0.064	100.45	0.0170
2-6	0.002	0.006	0.0015	Gly	1253.6	30	9.19E-04	8.50E-04	1.340	0.064	101.14	0.0178
2-6	0.002	0.006	0.0015	Gly	1253.6	45	9.27E-04	8.57E-04	1.340	0.064	105.00	0.0180
2-6	0.002	0.006	0.0015	Gly	1253.6	45	1.03E-03	9.53E-04	1.340	0.064	102.25	0.0200
2-6	0.002	0.006	0.0015	Gly	1253.6	30	1.21E-03	1.12E-03	1.340	0.064	103.25	0.0234
2-6	0.002	0.006	0.0015	Gly	1253.6	45	1.24E-03	1.15E-03	1.340	0.064	100.90	0.0240
2-6	0.002	0.006	0.0015	Gly	1253.6	45	1.26E-03	1.16E-03	1.340	0.064	105.20	0.0244
2-6	0.002	0.006	0.0015	Gly	1253.6	45	1.28E-03	1.18E-03	1.340	0.064	101.80	0.0248
2-6	0.002	0.006	0.0015	Gly	1253.6	60	1.31E-03	1.21E-03	1.340	0.064	103.75	0.0253
2-6	0.002	0.006	0.0015	Gly	1253.6	60	1.36E-03	1.26E-03	1.340	0.064	101.51	0.0263
2-6	0.002	0.006	0.0015	Gly	1253.6	60	1.36E-03	1.26E-03	1.340	0.064	104.60	0.0264

Table E2 (Continued)

Chamber (mm * mm)	Radius d (m)	Radius D (m)	Radius (m)	Liquid (name)	Density (kg/m^3)	Tilt (degree)	Velocity (m/s)	Velocity ADJUSTED	Viscosity (Pa.s)	S Tension (N/m)	DCA used	Ca ($\mu v/\gamma$)
2-6	0.002	0.006	0.0015	Gly	1253.6	45	1.44E-03	1.33E-03	1.340	0.064	97.00	0.0280
2-6	0.002	0.006	0.0015	Gly	1253.6	45	1.45E-03	1.34E-03	1.340	0.064	104.35	0.0281
2-6	0.002	0.006	0.0015	Gly	1253.6	60	1.70E-03	1.58E-03	1.340	0.064	102.15	0.0330
2-6	0.002	0.006	0.0015	Gly	1253.6	80	1.92E-03	1.77E-03	1.340	0.064	107.65	0.0371
2-6	0.002	0.006	0.0015	Gly	1253.6	60	1.93E-03	1.79E-03	1.340	0.064	105.00	0.0374
2-6	0.002	0.006	0.0015	Gly	1253.6	80	2.00E-03	1.85E-03	1.340	0.064	105.00	0.0388
9-3	0.0035	0.009	0.0025	Gly	1253.6	5	7.55E-05	6.99E-05	1.340	0.064	86.50	0.0015
9-3	0.0035	0.009	0.0025	Gly	1253.6	5	9.06E-05	8.38E-05	1.340	0.064	88.00	0.0018
9-3	0.0035	0.009	0.0025	Gly	1253.6	10	4.35E-04	4.02E-04	1.340	0.064	91.00	0.0084
9-3	0.0035	0.009	0.0025	Gly	1253.6	10	4.55E-04	4.21E-04	1.340	0.064	93.00	0.0088
9-3	0.0035	0.009	0.0025	Gly	1253.6	10	6.08E-04	5.62E-04	1.340	0.064	95.60	0.0118
9-3	0.0035	0.009	0.0025	Gly	1253.6	30	6.96E-04	6.43E-04	1.340	0.064	98.95	0.0135
9-3	0.0035	0.009	0.0025	Gly	1253.6	15	1.18E-03	1.09E-03	1.340	0.064	97.60	0.0228
9-3	0.0035	0.009	0.0025	Gly	1253.6	30	1.50E-03	1.39E-03	1.340	0.064	107.00	0.0291
9-3	0.0035	0.009	0.0025	Gly	1253.6	60	1.57E-03	1.45E-03	1.340	0.064	110.20	0.0304
9-3	0.0035	0.009	0.0025	Gly	1253.6	60	1.57E-03	1.45E-03	1.340	0.064	112.00	0.0304
9-3	0.0035	0.009	0.0025	Gly	1253.6	30	1.60E-03	1.48E-03	1.340	0.064	103.50	0.0309
9-3	0.0035	0.009	0.0025	Gly	1253.6	20	1.63E-03	1.50E-03	1.340	0.064	106.00	0.0315
9-3	0.0035	0.009	0.0025	Gly	1253.6	20	1.63E-03	1.50E-03	1.340	0.064	108.85	0.0315
9-3	0.0035	0.009	0.0025	Gly	1253.6	50	2.00E-03	1.85E-03	1.340	0.064	104.00	0.0388
9-3	0.0035	0.009	0.0025	Gly	1253.6	50	2.02E-03	1.87E-03	1.340	0.064	107.50	0.0391
9-3	0.0035	0.009	0.0025	Gly	1253.6	30	2.39E-03	2.21E-03	1.340	0.064	109.75	0.0464
9-3	0.0035	0.009	0.0025	Gly	1253.6	70	2.47E-03	2.29E-03	1.340	0.064	114.00	0.0479
9-3	0.0035	0.009	0.0025	Gly	1253.6	60	2.94E-03	2.72E-03	1.340	0.064	123.00	0.0569
9-3	0.0035	0.009	0.0025	Gly	1253.6	60	2.96E-03	2.74E-03	1.340	0.064	124.00	0.0573

Table E2 (Continued)

Chamber (mm * mm)	Radius d (m)	Radius D (m)	Radius (m)	Liquid (name)	Density (kg/m^3)	Tilt (degree)	Velocity (m/s)	Velocity ADJUSTED	Viscosity (Pa.s)	S Tension (N/m)	DCA used	Ca ($\mu v/\gamma$)
9-3	0.0035	0.009	0.0025	Gly	1253.6	70	3.20E-03	2.96E-03	1.340	0.064	124.00	0.0621
9-3	0.0035	0.009	0.0025	Gly	1253.6	70	3.20E-03	2.96E-03	1.340	0.064	127.00	0.0621
9-3	0.0035	0.009	0.0025	Gly	1253.6	80	3.90E-03	3.61E-03	1.340	0.064	123.60	0.0756
9-3	0.0035	0.009	0.0025	Gly	1253.6	80	3.90E-03	3.61E-03	1.340	0.064	120.90	0.0756
9-3	0.0035	0.009	0.0025	Gly	1253.6	65	4.01E-03	3.71E-03	1.340	0.064	128.00	0.0776
9-3	0.0035	0.009	0.0025	Gly	1253.6	65	4.01E-03	3.71E-03	1.340	0.064	124.50	0.0776
9-3	0.0035	0.009	0.0025	Gly	1253.6	45	4.50E-03	4.16E-03	1.340	0.064	115.70	0.0871
9-3	0.0035	0.009	0.0025	Gly	1253.6	45	4.50E-03	4.16E-03	1.340	0.064	113.50	0.0871
9-3	0.0035	0.009	0.0025	Gly	1253.6	75	5.93E-03	5.48E-03	1.340	0.064	129.00	0.1148
9-3	0.0035	0.009	0.0025	Gly	1253.6	75	5.93E-03	5.48E-03	1.340	0.064	126.00	0.1148
9-3	0.0035	0.009	0.0025	Gly	1253.6	60	6.01E-03	5.56E-03	1.340	0.064	127.00	0.1165
9-3	0.0035	0.009	0.0025	Gly	1253.6	60	6.01E-03	5.56E-03	1.340	0.064	125.36	0.1165
9-3	0.0035	0.009	0.0025	V100000	999.6	3	2.08E-06	1.92E-06	104.32	0.0225	61.00	0.0089
9-3	0.0035	0.009	0.0025	V100000	999.6	3	2.08E-06	1.92E-06	104.32	0.0225	59.45	0.0089
9-3	0.0035	0.009	0.0025	V100000	999.6	5	3.92E-06	3.63E-06	104.32	0.0225	63.40	0.0168
9-3	0.0035	0.009	0.0025	V100000	999.6	5	3.92E-06	3.63E-06	104.32	0.0225	61.93	0.0168
9-3	0.0035	0.009	0.0025	V100000	999.6	10	7.04E-06	6.51E-06	104.32	0.0225	82.00	0.0302
9-3	0.0035	0.009	0.0025	V100000	999.6	10	7.04E-06	6.51E-06	104.32	0.0225	78.25	0.0302
9-3	0.0035	0.009	0.0025	V100000	999.6	10	8.77E-06	8.11E-06	104.32	0.0225	79.00	0.0376
9-3	0.0035	0.009	0.0025	V100000	999.6	10	8.77E-06	8.11E-06	104.32	0.0225	76.88	0.0376
9-3	0.0035	0.009	0.0025	V100000	999.6	10	8.86E-06	8.19E-06	104.32	0.0225	81.22	0.0380
9-3	0.0035	0.009	0.0025	V100000	999.6	10	8.86E-06	8.19E-06	104.32	0.0225	81.70	0.0380
9-3	0.0035	0.009	0.0025	V100000	999.6	15	1.32E-05	1.22E-05	104.32	0.0225	87.25	0.0567
9-3	0.0035	0.009	0.0025	V100000	999.6	20	1.71E-05	1.58E-05	104.32	0.0225	95.45	0.0731
9-3	0.0035	0.009	0.0025	V100000	999.6	25	1.98E-05	1.83E-05	104.32	0.0225	96.70	0.0848

Table E2 (Continued)

Chamber (mm * mm)	Radius d (m)	Radius D (m)	Radius (m)	Liquid (name)	Density (kg/m^3)	Tilt (degree)	Velocity (m/s)	Velocity ADJUSTED	Viscosity (Pa.s)	S Tension (N/m)	DCA used	Ca ($\mu v/\gamma$)
9-3	0.0035	0.009	0.0025	V100000	999.6	20	2.08E-05	1.92E-05	104.32	0.0225	92.25	0.0891
9-3	0.0035	0.009	0.0025	V100000	999.6	30	2.38E-05	2.20E-05	104.32	0.0225	104.00	0.1020
9-3	0.0035	0.009	0.0025	V100000	999.6	30	2.38E-05	2.20E-05	104.32	0.0225	102.70	0.1020
9-3	0.0035	0.009	0.0025	V100000	999.6	30	2.39E-05	2.21E-05	104.32	0.0225	105.00	0.1026
9-3	0.0035	0.009	0.0025	V100000	999.6	30	2.39E-05	2.21E-05	104.32	0.0225	102.50	0.1026
9-3	0.0035	0.009	0.0025	V100000	999.6	40	2.61E-05	2.41E-05	104.32	0.0225	107.22	0.1119
9-3	0.0035	0.009	0.0025	V100000	999.6	45	3.22E-05	2.98E-05	104.32	0.0225	119.00	0.1383
9-3	0.0035	0.009	0.0025	V100000	999.6	45	3.22E-05	2.98E-05	104.32	0.0225	115.75	0.1383
9-3	0.0035	0.009	0.0025	V100000	999.6	50	3.23E-05	2.99E-05	104.32	0.0225	113.25	0.1385
9-3	0.0035	0.009	0.0025	V100000	999.6	70	3.25E-05	3.01E-05	104.32	0.0225	128.50	0.1394
9-3	0.0035	0.009	0.0025	V100000	999.6	35	3.38E-05	3.13E-05	104.32	0.0225	115.00	0.1451
9-3	0.0035	0.009	0.0025	V100000	999.6	35	3.38E-05	3.13E-05	104.32	0.0225	111.30	0.1451
9-3	0.0035	0.009	0.0025	V100000	999.6	45	3.44E-05	3.18E-05	104.32	0.0225	123.10	0.1475
9-3	0.0035	0.009	0.0025	V100000	999.6	45	3.44E-05	3.18E-05	104.32	0.0225	121.05	0.1475
9-3	0.0035	0.009	0.0025	V100000	999.6	55	3.68E-05	3.40E-05	104.32	0.0225	126.25	0.1577
9-3	0.0035	0.009	0.0025	V100000	999.6	55	3.73E-05	3.45E-05	104.32	0.0225	132.50	0.1601
9-3	0.0035	0.009	0.0025	V100000	999.6	55	3.72E-05	3.44E-05	104.32	0.0225	121.75	0.1597
9-3	0.0035	0.009	0.0025	V100000	999.6	60	3.86E-05	3.57E-05	104.32	0.0225	125.20	0.1656
9-3	0.0035	0.009	0.0025	V100000	999.6	60	3.86E-05	3.57E-05	104.32	0.0225	121.85	0.1656
9-3	0.0035	0.009	0.0025	V100000	999.6	70	3.93E-05	3.63E-05	104.32	0.0225	131.50	0.1684
9-3	0.0035	0.009	0.0025	V100000	999.6	70	3.95E-05	3.65E-05	104.32	0.0225	135.00	0.1693
9-3	0.0035	0.009	0.0025	V100000	999.6	75	3.98E-05	3.68E-05	104.32	0.0225	141.50	0.1707
9-3	0.0035	0.009	0.0025	V100000	999.6	75	3.98E-05	3.68E-05	104.32	0.0225	140.75	0.1707
9-3	0.0035	0.009	0.0025	V100000	999.6	80	4.09E-05	3.78E-05	104.32	0.0225	135.00	0.1754
9-3	0.0035	0.009	0.0025	V100000	999.6	80	4.11E-05	3.80E-05	104.32	0.0225	134.20	0.1762

Table E2 (Continued)

Chamber (mm * mm)	Radius d (m)	Radius D (m)	Radius (m)	Liquid (name)	Density (kg/m^3)	Tilt (degree)	Velocity (m/s)	Velocity ADJUSTED	Viscosity (Pa.s)	S Tension (N/m)	DCA used	Ca ($\mu v/\gamma$)
9-3	0.0035	0.009	0.0025	V100000	999.6	70	4.11E-05	3.80E-05	104.32	0.0225	131.04	0.1763
9-3	0.0035	0.009	0.0025	V100000	999.6	70	4.21E-05	3.89E-05	104.32	0.0225	133.00	0.1806
9-3	0.0035	0.009	0.0025	V100000	999.6	80	4.29E-05	3.97E-05	104.32	0.0225	145.00	0.1840
9-3	0.0035	0.009	0.0025	V100000	999.6	75	4.34E-05	4.02E-05	104.32	0.0225	135.00	0.1862
9-3	0.0035	0.009	0.0025	V100000	999.6	85	4.66E-05	4.31E-05	104.32	0.0225	134.00	0.1999
10-15	0.0039	0.012	0.0029	V100000	999.6	1	1.87E-06	1.73E-06	104.32	0.0225	52.50	0.0080
10-15	0.0039	0.012	0.0029	V100000	999.6	6.8	8.54E-06	7.90E-06	104.32	0.0225	80.55	0.0366
10-15	0.0039	0.012	0.0029	V100000	999.6	6	1.21E-05	1.12E-05	104.32	0.0225	77.15	0.0518
10-15	0.0039	0.012	0.0029	V100000	999.6	10	1.36E-05	1.26E-05	104.32	0.0225	88.85	0.0585
10-15	0.0039	0.012	0.0029	V100000	999.6	10	1.69E-05	1.57E-05	104.32	0.0225	92.10	0.0727
10-15	0.0039	0.012	0.0029	V100000	999.6	15	1.96E-05	1.82E-05	104.32	0.0225	96.55	0.0842
10-15	0.0039	0.012	0.0029	V100000	999.6	20	2.48E-05	2.29E-05	104.32	0.0225	102.50	0.1064
10-15	0.0039	0.012	0.0029	V100000	999.6	20	2.69E-05	2.49E-05	104.32	0.0225	103.50	0.1152
10-15	0.0039	0.012	0.0029	V100000	999.6	30	2.84E-05	2.63E-05	104.32	0.0225	109.50	0.1219
10-15	0.0039	0.012	0.0029	V100000	999.6	26	3.31E-05	3.06E-05	104.32	0.0225	122.00	0.1418
2-6	0.002	0.006	0.0015	V30000	1002.3	5	5.25E-06	4.85E-06	30.880	0.022	66.15	0.0068
2-6	0.002	0.006	0.0015	V30000	1002.3	5	6.79E-06	6.28E-06	30.880	0.022	56.50	0.0088
2-6	0.002	0.006	0.0015	V30000	1002.3	5	6.88E-06	6.36E-06	30.880	0.022	69.67	0.0089
2-6	0.002	0.006	0.0015	V30000	1002.3	10	7.73E-06	7.15E-06	30.880	0.022	69.00	0.0100
2-6	0.002	0.006	0.0015	V30000	1002.3	15	9.93E-06	9.18E-06	30.880	0.022	80.65	0.0129
2-6	0.002	0.006	0.0015	V30000	1002.3	10	1.29E-05	1.20E-05	30.880	0.022	70.00	0.0168
2-6	0.002	0.006	0.0015	V30000	1002.3	10	1.33E-05	1.23E-05	30.880	0.022	81.71	0.0173
2-6	0.002	0.006	0.0015	V30000	1002.3	15	1.66E-05	1.53E-05	30.880	0.022	73.00	0.0215
2-6	0.002	0.006	0.0015	V30000	1002.3	15	1.66E-05	1.53E-05	30.880	0.022	77.00	0.0215
2-6	0.002	0.006	0.0015	V30000	1002.3	20	2.05E-05	1.90E-05	30.880	0.022	90.05	0.0266

Table E2 (Continued)

Chamber (mm * mm)	Radius d (m)	Radius D (m)	Radius (m)	Liquid (name)	Density (kg/m^3)	Tilt (degree)	Velocity (m/s)	Velocity ADJUSTED	Viscosity (Pa.s)	S Tension (N/m)	DCA used	Ca ($\mu v/\gamma$)
2-6	0.002	0.006	0.0015	V30000	1002.3	20	2.45E-05	2.26E-05	30.880	0.022	74.00	0.0318
2-6	0.002	0.006	0.0015	V30000	1002.3	20	2.45E-05	2.26E-05	30.880	0.022	76.08	0.0318
2-6	0.002	0.006	0.0015	V30000	1002.3	30	2.80E-05	2.59E-05	30.880	0.022	91.90	0.0364
2-6	0.002	0.006	0.0015	V30000	1002.3	35	2.97E-05	2.75E-05	30.880	0.022	94.40	0.0386
2-6	0.002	0.006	0.0015	V30000	1002.3	30	3.17E-05	2.93E-05	30.880	0.022	92.57	0.0412
2-6	0.002	0.006	0.0015	V30000	1002.3	50	3.54E-05	3.28E-05	30.880	0.022	102.75	0.0460
2-6	0.002	0.006	0.0015	V30000	1002.3	40	3.65E-05	3.38E-05	30.880	0.022	88.00	0.0474
2-6	0.002	0.006	0.0015	V30000	1002.3	60	4.00E-05	3.70E-05	30.880	0.022	100.85	0.0519
2-6	0.002	0.006	0.0015	V30000	1002.3	45	4.09E-05	3.79E-05	30.880	0.022	95.00	0.0531
2-6	0.002	0.006	0.0015	V30000	1002.3	45	4.20E-05	3.89E-05	30.880	0.022	96.55	0.0546
2-6	0.002	0.006	0.0015	V30000	1002.3	70	4.00E-05	3.70E-05	30.880	0.022	103.40	0.0520
2-6	0.002	0.006	0.0015	V30000	1002.3	60	5.28E-05	4.88E-05	30.880	0.022	100.84	0.0685
2-6	0.002	0.006	0.0015	V30000	1002.3	60	5.33E-05	4.93E-05	30.880	0.022	101.50	0.0692
2-6	0.002	0.006	0.0015	V30000	1002.3	80	5.79E-05	5.36E-05	30.880	0.022	96.40	0.0752
2-6	0.002	0.006	0.0015	V30000	1002.3	80	5.90E-05	5.45E-05	30.880	0.022	103.50	0.0765
2-6	0.002	0.006	0.0015	V30000	1002.3	80	6.56E-05	6.07E-05	30.880	0.022	103.12	0.0852
9-3	0.0035	0.009	0.0025	V30000	1002.3	5	1.30E-05	1.20E-05	30.88	0.022	73.00	0.0169
9-3	0.0035	0.009	0.0025	V30000	1002.3	2.5	1.32E-05	1.23E-05	30.88	0.022	69.05	0.0172
9-3	0.0035	0.009	0.0025	V30000	1002.3	5	1.43E-05	1.33E-05	30.88	0.022	72.90	0.0186
9-3	0.0035	0.009	0.0025	V30000	1002.3	10	2.60E-05	2.40E-05	30.88	0.022	83.20	0.0337
9-3	0.0035	0.009	0.0025	V30000	1002.3	10	2.79E-05	2.58E-05	30.88	0.022	87.85	0.0362
9-3	0.0035	0.009	0.0025	V30000	1002.3	10	3.14E-05	2.90E-05	30.88	0.022	89.00	0.0407
9-3	0.0035	0.009	0.0025	V30000	1002.3	15	3.24E-05	2.99E-05	30.88	0.022	89.10	0.0420
9-3	0.0035	0.009	0.0025	V30000	1002.3	20	4.88E-05	4.52E-05	30.88	0.022	97.95	0.0634
9-3	0.0035	0.009	0.0025	V30000	1002.3	25	5.04E-05	4.66E-05	30.88	0.022	100.09	0.0654

Table E2 (Continued)

Chamber (mm * mm)	Radius d (m)	Radius D (m)	Radius (m)	Liquid (name)	Density (kg/m^3)	Tilt (degree)	Velocity (m/s)	Velocity ADJUSTED	Viscosity (Pa.s)	S Tension (N/m)	DCA used	Ca ($\mu v/\gamma$)
9-3	0.0035	0.009	0.0025	V30000	1002.3	20	5.38E-05	4.97E-05	30.88	0.022	98.05	0.0698
9-3	0.0035	0.009	0.0025	V30000	1002.3	20	5.46E-05	5.05E-05	30.88	0.022	97.10	0.0708
9-3	0.0035	0.009	0.0025	V30000	1002.3	40	6.36E-05	5.88E-05	30.88	0.022	101.15	0.0825
9-3	0.0035	0.009	0.0025	V30000	1002.3	30	6.75E-05	6.25E-05	30.88	0.022	105.20	0.0877
9-3	0.0035	0.009	0.0025	V30000	1002.3	30	7.23E-05	6.69E-05	30.88	0.022	104.13	0.0939
9-3	0.0035	0.009	0.0025	V30000	1002.3	40	8.45E-05	7.82E-05	30.88	0.022	109.30	0.1098
9-3	0.0035	0.009	0.0025	V30000	1002.3	40	8.55E-05	7.91E-05	30.88	0.022	114.80	0.1110
9-3	0.0035	0.009	0.0025	V30000	1002.3	45	9.07E-05	8.39E-05	30.88	0.022	117.50	0.1177
9-3	0.0035	0.009	0.0025	V30000	1002.3	60	9.48E-05	8.77E-05	30.88	0.022	140.50	0.1231
9-3	0.0035	0.009	0.0025	V30000	1002.3	50	9.95E-05	9.21E-05	30.88	0.022	118.30	0.1292
9-3	0.0035	0.009	0.0025	V30000	1002.3	50	9.95E-05	9.21E-05	30.88	0.022	118.64	0.1292
9-3	0.0035	0.009	0.0025	V30000	1002.3	45	1.06E-04	9.83E-05	30.88	0.022	120.40	0.1379
9-3	0.0035	0.009	0.0025	V30000	1002.3	45	1.06E-04	9.83E-05	30.88	0.022	117.50	0.1379
9-3	0.0035	0.009	0.0025	V30000	1002.3	60	1.06E-04	9.84E-05	30.88	0.022	125.55	0.1381
9-3	0.0035	0.009	0.0025	V30000	1002.3	45	1.07E-04	9.90E-05	30.88	0.022	123.65	0.1390
9-3	0.0035	0.009	0.0025	V30000	1002.3	60	1.09E-04	1.01E-04	30.88	0.022	121.55	0.1411
9-3	0.0035	0.009	0.0025	V30000	1002.3	50	1.10E-04	1.01E-04	30.88	0.022	120.25	0.1422
9-3	0.0035	0.009	0.0025	V30000	1002.3	50	1.11E-04	1.03E-04	30.88	0.022	123.00	0.1441
9-3	0.0035	0.009	0.0025	V30000	1002.3	60	1.12E-04	1.04E-04	30.88	0.022	128.00	0.1455
9-3	0.0035	0.009	0.0025	V30000	1002.3	70	1.15E-04	1.06E-04	30.88	0.022	140.65	0.1490
9-3	0.0035	0.009	0.0025	V30000	1002.3	60	1.18E-04	1.09E-04	30.88	0.022	119.11	0.1534
9-3	0.0035	0.009	0.0025	V30000	1002.3	70	1.22E-04	1.13E-04	30.88	0.022	162.80	0.1590
9-3	0.0035	0.009	0.0025	V30000	1002.3	85	1.24E-04	1.15E-04	30.88	0.022	139.35	0.1610
9-3	0.0035	0.009	0.0025	V30000	1002.3	60	1.29E-04	1.19E-04	30.88	0.022	126.00	0.1670
9-3	0.0035	0.009	0.0025	V30000	1002.3	60	1.32E-04	1.22E-04	30.88	0.022	123.60	0.1711

Table E2 (Continued)

Chamber (mm * mm)	Radius d (m)	Radius D (m)	Radius (m)	Liquid (name)	Density (kg/m^3)	Tilt (degree)	Velocity (m/s)	Velocity ADJUSTED	Viscosity (Pa.s)	S Tension (N/m)	DCA used	Ca ($\mu v/\gamma$)
9-3	0.0035	0.009	0.0025	V30000	1002.3	80	1.33E-04	1.23E-04	30.88	0.022	123.20	0.1727
9-3	0.0035	0.009	0.0025	V30000	1002.3	60	1.36E-04	1.26E-04	30.88	0.022	126.50	0.1771
9-3	0.0035	0.009	0.0025	V30000	1002.3	85	1.51E-04	1.40E-04	30.88	0.022	138.00	0.1959
9-3	0.0035	0.009	0.0025	V30000	1002.3	85	1.52E-04	1.41E-04	30.88	0.022	164.00	0.1972
10-15	0.0039	0.012	0.0029	V30000	1002.3	1	2.84E-06	2.63E-06	30.88	0.022	40.05	0.0037
10-15	0.0039	0.012	0.0029	V30000	1002.3	1	2.99E-06	2.77E-06	30.88	0.022	52.98	0.0039
10-15	0.0039	0.012	0.0029	V30000	1002.3	1	3.77E-06	3.49E-06	30.88	0.022	44.95	0.0049
10-15	0.0039	0.012	0.0029	V30000	1002.3	1	3.85E-06	3.56E-06	30.88	0.022	50.99	0.0050
10-15	0.0039	0.012	0.0029	V30000	1002.3	1	9.40E-06	8.69E-06	30.88	0.022	78.39	0.0122
10-15	0.0039	0.012	0.0029	V30000	1002.3	5	1.75E-05	1.62E-05	30.88	0.022	83.60	0.0227
10-15	0.0039	0.012	0.0029	V30000	1002.3	15	2.66E-05	2.46E-05	30.88	0.022	90.00	0.0345
10-15	0.0039	0.012	0.0029	V30000	1002.3	10	2.76E-05	2.55E-05	30.88	0.022	90.00	0.0358
10-15	0.0039	0.012	0.0029	V30000	1002.3	5	3.31E-05	3.06E-05	30.88	0.022	83.24	0.0429
10-15	0.0039	0.012	0.0029	V30000	1002.3	5	3.31E-05	3.06E-05	30.88	0.022	73.50	0.0429
10-15	0.0039	0.012	0.0029	V30000	1002.3	20	4.42E-05	4.09E-05	30.88	0.022	102.00	0.0574
10-15	0.0039	0.012	0.0029	V30000	1002.3	10	4.46E-05	4.13E-05	30.88	0.022	94.30	0.0580
10-15	0.0039	0.012	0.0029	V30000	1002.3	10	5.37E-05	4.97E-05	30.88	0.022	94.29	0.0698
10-15	0.0039	0.012	0.0029	V30000	1002.3	5	5.48E-05	5.07E-05	30.88	0.022	78.05	0.0711
10-15	0.0039	0.012	0.0029	V30000	1002.3	20	6.82E-05	6.31E-05	30.88	0.022	96.05	0.0885
10-15	0.0039	0.012	0.0029	V30000	1002.3	30	8.40E-05	7.77E-05	30.88	0.022	107.79	0.1091
10-15	0.0039	0.012	0.0029	V30000	1002.3	30	8.40E-05	7.77E-05	30.88	0.022	109.25	0.1091
10-15	0.0039	0.012	0.0029	V30000	1002.3	45	1.30E-04	1.20E-04	30.88	0.022	128.50	0.1691
10-15	0.0039	0.012	0.0029	V30000	1002.3	45	1.43E-04	1.32E-04	30.88	0.022	153.80	0.1857
2-6	0.002	0.006	0.0015	V500	975.2	5	2.10E-04	1.95E-04	0.486	0.024	65.75	0.0039
2-6	0.002	0.006	0.0015	V500	975.2	5	2.15E-04	1.99E-04	0.486	0.024	57.90	0.0040

Table E2 (Continued)

Chamber (mm * mm)	Radius d (m)	Radius D (m)	Radius (m)	Liquid (name)	Density (kg/m^3)	Tilt (degree)	Velocity (m/s)	Velocity ADJUSTED	Viscosity (Pa.s)	S Tension (N/m)	DCA used	Ca ($\mu v/\gamma$)
2-6	0.002	0.006	0.0015	V500	975.2	5	2.52E-04	2.33E-04	0.486	0.024	63.90	0.0047
2-6	0.002	0.006	0.0015	V500	975.2	10	3.25E-04	3.00E-04	0.486	0.024	62.50	0.0061
2-6	0.002	0.006	0.0015	V500	975.2	5	3.88E-04	3.59E-04	0.486	0.024	68.70	0.0073
2-6	0.002	0.006	0.0015	V500	975.2	10	4.46E-04	4.13E-04	0.486	0.024	72.00	0.0084
2-6	0.002	0.006	0.0015	V500	975.2	10	4.66E-04	4.31E-04	0.486	0.024	70.15	0.0087
2-6	0.002	0.006	0.0015	V500	975.2	15	4.93E-04	4.56E-04	0.486	0.024	69.00	0.0092
2-6	0.002	0.006	0.0015	V500	975.2	10	4.96E-04	4.59E-04	0.486	0.024	70.80	0.0093
2-6	0.002	0.006	0.0015	V500	975.2	20	6.42E-04	5.93E-04	0.486	0.024	73.50	0.0120
2-6	0.002	0.006	0.0015	V500	975.2	25	6.68E-04	6.18E-04	0.486	0.024	76.43	0.0125
2-6	0.002	0.006	0.0015	V500	975.2	20	9.06E-04	8.38E-04	0.486	0.024	89.50	0.0170
2-6	0.002	0.006	0.0015	V500	975.2	30	9.10E-04	8.41E-04	0.486	0.024	78.00	0.0170
2-6	0.002	0.006	0.0015	V500	975.2	15	9.31E-04	8.61E-04	0.486	0.024	85.25	0.0174
2-6	0.002	0.006	0.0015	V500	975.2	20	1.00E-03	9.28E-04	0.486	0.024	86.25	0.0188
2-6	0.002	0.006	0.0015	V500	975.2	20	1.08E-03	9.99E-04	0.486	0.024	85.40	0.0202
2-6	0.002	0.006	0.0015	V500	975.2	40	1.09E-03	1.01E-03	0.486	0.024	81.40	0.0205
2-6	0.002	0.006	0.0015	V500	975.2	50	1.25E-03	1.16E-03	0.486	0.024	81.60	0.0235
2-6	0.002	0.006	0.0015	V500	975.2	70	1.29E-03	1.19E-03	0.486	0.024	87.50	0.0241
2-6	0.002	0.006	0.0015	V500	975.2	30	1.43E-03	1.33E-03	0.486	0.024	89.05	0.0269
2-6	0.002	0.006	0.0015	V500	975.2	30	1.52E-03	1.41E-03	0.486	0.024	92.55	0.0285
2-6	0.002	0.006	0.0015	V500	975.2	80	1.56E-03	1.44E-03	0.486	0.024	90.00	0.0291
2-6	0.002	0.006	0.0015	V500	975.2	60	1.57E-03	1.45E-03	0.486	0.024	90.40	0.0294
2-6	0.002	0.006	0.0015	V500	975.2	30	1.75E-03	1.62E-03	0.486	0.024	91.90	0.0328
2-6	0.002	0.006	0.0015	V500	975.2	30	1.76E-03	1.63E-03	0.486	0.024	93.05	0.0330
2-6	0.002	0.006	0.0015	V500	975.2	45	1.87E-03	1.73E-03	0.486	0.024	101.00	0.0351
2-6	0.002	0.006	0.0015	V500	975.2	50	2.23E-03	2.07E-03	0.486	0.024	98.95	0.0418

Table E2 (Continued)

Chamber (mm * mm)	Radius d (m)	Radius D (m)	Radius (m)	Liquid (name)	Density (kg/m^3)	Tilt (degree)	Velocity (m/s)	Velocity ADJUSTED	Viscosity (Pa.s)	S Tension (N/m)	DCA used	Ca ($\mu v/\gamma$)
2-6	0.002	0.006	0.0015	V500	975.2	45	2.33E-03	2.15E-03	0.486	0.024	96.50	0.0436
2-6	0.002	0.006	0.0015	V500	975.2	70	2.47E-03	2.29E-03	0.486	0.024	102.50	0.0463
2-6	0.002	0.006	0.0015	V500	975.2	45	2.59E-03	2.40E-03	0.486	0.024	99.20	0.0485
2-6	0.002	0.006	0.0015	V500	975.2	45	2.64E-03	2.45E-03	0.486	0.024	100.50	0.0495
2-6	0.002	0.006	0.0015	V500	975.2	60	2.79E-03	2.58E-03	0.486	0.024	100.66	0.0522
2-6	0.002	0.006	0.0015	V500	975.2	60	2.85E-03	2.64E-03	0.486	0.024	105.50	0.0534
2-6	0.002	0.006	0.0015	V500	975.2	60	2.88E-03	2.66E-03	0.486	0.024	101.50	0.0539
2-6	0.002	0.006	0.0015	V500	975.2	80	3.10E-03	2.87E-03	0.486	0.024	108.50	0.0581
2-6	0.002	0.006	0.0015	V500	975.2	80	3.23E-03	2.98E-03	0.486	0.024	100.80	0.0604
2-6	0.002	0.006	0.0015	V500	975.2	60	3.28E-03	3.03E-03	0.486	0.024	105.00	0.0614
2-6	0.002	0.006	0.0015	V500	975.2	85	3.79E-03	3.50E-03	0.486	0.024	105.00	0.0709
2-6	0.002	0.006	0.0015	V500	975.2	80	4.12E-03	3.81E-03	0.486	0.024	104.10	0.0772
9-3	0.0035	0.009	0.0025	V500	975.2	1	8.27E-05	7.65E-05	0.486	0.024	39.57	0.0015
9-3	0.0035	0.009	0.0025	V500	975.2	1	8.27E-05	7.65E-05	0.486	0.024	43.50	0.0015
9-3	0.0035	0.009	0.0025	V500	975.2	5	5.29E-04	4.89E-04	0.486	0.024	70.50	0.0099
9-3	0.0035	0.009	0.0025	V500	975.2	5	5.36E-04	4.96E-04	0.486	0.024	64.70	0.0100
9-3	0.0035	0.009	0.0025	V500	975.2	5	5.59E-04	5.17E-04	0.486	0.024	76.30	0.0105
9-3	0.0035	0.009	0.0025	V500	975.2	5	6.10E-04	5.64E-04	0.486	0.024	71.10	0.0114
9-3	0.0035	0.009	0.0025	V500	975.2	10	1.19E-03	1.10E-03	0.486	0.024	86.90	0.0224
9-3	0.0035	0.009	0.0025	V500	975.2	10	1.38E-03	1.28E-03	0.486	0.024	87.65	0.0259
9-3	0.0035	0.009	0.0025	V500	975.2	15	1.90E-03	1.76E-03	0.486	0.024	97.00	0.0356
9-3	0.0035	0.009	0.0025	V500	975.2	15	2.60E-03	2.41E-03	0.486	0.024	99.00	0.0488
9-3	0.0035	0.009	0.0025	V500	975.2	30	3.54E-03	3.27E-03	0.486	0.024	112.85	0.0663
9-3	0.0035	0.009	0.0025	V500	975.2	30	3.86E-03	3.57E-03	0.486	0.024	117.00	0.0723
9-3	0.0035	0.009	0.0025	V500	975.2	30	3.86E-03	3.57E-03	0.486	0.024	114.00	0.0724

Table E2 (Continued)

Chamber (mm * mm)	Radius d (m)	Radius D (m)	Radius (m)	Liquid (name)	Density (kg/m^3)	Tilt (degree)	Velocity (m/s)	Velocity ADJUSTED	Viscosity (Pa.s)	S Tension (N/m)	DCA used	Ca ($\mu v/\gamma$)
9-3	0.0035	0.009	0.0025	V500	975.2	30	4.59E-03	4.24E-03	0.486	0.024	117.56	0.0860
9-3	0.0035	0.009	0.0025	V500	975.2	30	4.88E-03	4.52E-03	0.486	0.024	115.50	0.0915
9-3	0.0035	0.009	0.0025	V500	975.2	40	5.40E-03	5.00E-03	0.486	0.024	128.05	0.1012
9-3	0.0035	0.009	0.0025	V500	975.2	50	6.73E-03	6.23E-03	0.486	0.024	141.75	0.1261
9-3	0.0035	0.009	0.0025	V500	975.2	45	7.52E-03	6.95E-03	0.486	0.024	151.00	0.1408
9-3	0.0035	0.009	0.0025	V500	975.2	60	7.91E-03	7.31E-03	0.486	0.024	163.40	0.1481
2-4	0.002	0.004	0.0013	V100	966.4	5	1.24E-03	1.14E-03	0.0968	0.0227	61.50	0.0049
2-4	0.002	0.004	0.0013	V100	966.4	15	3.73E-03	3.45E-03	0.0968	0.0227	85.70	0.0147
2-4	0.002	0.004	0.0013	V100	966.4	30	1.78E-03	1.65E-03	0.0968	0.0227	65.56	0.0070
2-4	0.002	0.004	0.0013	V100	966.4	30	8.44E-03	7.80E-03	0.0968	0.0227	90.00	0.0333
2-4	0.002	0.004	0.0013	V100	966.4	30	1.03E-02	9.52E-03	0.0968	0.0227	89.91	0.0406
2-4	0.002	0.004	0.0013	V100	966.4	30	1.08E-02	9.99E-03	0.0968	0.0227	89.16	0.0426
2-4	0.002	0.004	0.0013	V100	966.4	30	1.14E-02	1.06E-02	0.0968	0.0227	90.96	0.0451
2-4	0.002	0.004	0.0013	V100	966.4	40	8.21E-03	7.59E-03	0.0968	0.0227	88.15	0.0324
2-4	0.002	0.004	0.0013	V100	966.4	45	3.50E-03	3.24E-03	0.0968	0.0227	74.72	0.0138
2-4	0.002	0.004	0.0013	V100	966.4	60	1.27E-02	1.17E-02	0.0968	0.0227	95.78	0.0499
2-4	0.002	0.004	0.0013	V100	966.4	60	1.47E-02	1.36E-02	0.0968	0.0227	96.00	0.0582
2-4	0.002	0.004	0.0013	V100	966.4	60	1.86E-02	1.72E-02	0.0968	0.0227	103.38	0.0732
2-4	0.002	0.004	0.0013	V100	966.4	60	1.87E-02	1.73E-02	0.0968	0.0227	100.17	0.0737
2-4	0.002	0.004	0.0013	V100	966.4	60	2.07E-02	1.91E-02	0.0968	0.0227	112.45	0.0815
2-4	0.002	0.004	0.0013	V100	966.4	70	1.44E-02	1.34E-02	0.0968	0.0227	98.50	0.0570
2-4	0.002	0.004	0.0013	V100	966.4	70	1.80E-02	1.67E-02	0.0968	0.0227	102.25	0.0711
2-4	0.002	0.004	0.0013	V100	966.4	80	1.60E-02	1.48E-02	0.0968	0.0227	97.19	0.0631
2-4	0.002	0.004	0.0013	V100	966.4	80	2.12E-02	1.96E-02	0.0968	0.0227	104.50	0.0836
2-4	0.002	0.004	0.0013	V100	966.4	80	2.18E-02	2.01E-02	0.0968	0.0227	117.21	0.0859

Table E2 (Continued)

Chamber (mm * mm)	Radius d (m)	Radius D (m)	Radius (m)	Liquid (name)	Density (kg/m^3)	Tilt (degree)	Velocity (m/s)	Velocity ADJUSTED	Viscosity (Pa.s)	S Tension (N/m)	DCA used	Ca ($\mu v/\gamma$)
2-6	0.002	0.006	0.0015	V100	966.4	5	8.32E-04	7.70E-04	0.0968	0.0227	58.10	0.0033
2-6	0.002	0.006	0.0015	V100	966.4	10	1.76E-03	1.63E-03	0.0968	0.0227	72.50	0.0069
2-6	0.002	0.006	0.0015	V100	966.4	10	2.85E-03	2.64E-03	0.0968	0.0227	74.35	0.0112
2-6	0.002	0.006	0.0015	V100	966.4	20	5.56E-03	5.14E-03	0.0968	0.0227	88.35	0.0219
2-6	0.002	0.006	0.0015	V100	966.4	30	5.84E-03	5.40E-03	0.0968	0.0227	80.80	0.0230
2-6	0.002	0.006	0.0015	V100	966.4	60	6.73E-03	6.22E-03	0.0968	0.0227	94.85	0.0265
2-6	0.002	0.006	0.0015	V100	966.4	30	7.58E-03	7.01E-03	0.0968	0.0227	90.42	0.0299
2-6	0.002	0.006	0.0015	V100	966.4	30	7.80E-03	7.22E-03	0.0968	0.0227	95.50	0.0308
2-6	0.002	0.006	0.0015	V100	966.4	45	8.51E-03	7.87E-03	0.0968	0.0227	90.61	0.0336
2-6	0.002	0.006	0.0015	V100	966.4	30	9.83E-03	9.09E-03	0.0968	0.0227	92.88	0.0388
2-6	0.002	0.006	0.0015	V100	966.4	60	9.87E-03	9.13E-03	0.0968	0.0227	101.80	0.0389
2-6	0.002	0.006	0.0015	V100	966.4	30	9.88E-03	9.14E-03	0.0968	0.0227	91.32	0.0390
2-6	0.002	0.006	0.0015	V100	966.4	30	1.04E-02	9.65E-03	0.0968	0.0227	94.10	0.0412
2-6	0.002	0.006	0.0015	V100	966.4	45	1.10E-02	1.02E-02	0.0968	0.0227	95.97	0.0435
2-6	0.002	0.006	0.0015	V100	966.4	70	1.12E-02	1.03E-02	0.0968	0.0227	103.50	0.0441
2-6	0.002	0.006	0.0015	V100	966.4	40	1.12E-02	1.04E-02	0.0968	0.0227	98.00	0.0443
2-6	0.002	0.006	0.0015	V100	966.4	80	1.37E-02	1.27E-02	0.0968	0.0227	114.00	0.0541
2-6	0.002	0.006	0.0015	V100	966.4	60	1.39E-02	1.29E-02	0.0968	0.0227	108.00	0.0549
2-6	0.002	0.006	0.0015	V100	966.4	60	1.43E-02	1.32E-02	0.0968	0.0227	99.45	0.0565
2-6	0.002	0.006	0.0015	V100	966.4	45	1.44E-02	1.33E-02	0.0968	0.0227	97.92	0.0567
2-6	0.002	0.006	0.0015	V100	966.4	45	1.46E-02	1.35E-02	0.0968	0.0227	98.75	0.0575
2-6	0.002	0.006	0.0015	V100	966.4	80	1.47E-02	1.36E-02	0.0968	0.0227	101.35	0.0580
2-6	0.002	0.006	0.0015	V100	966.4	45	1.57E-02	1.45E-02	0.0968	0.0227	98.81	0.0619
2-6	0.002	0.006	0.0015	V100	966.4	60	1.67E-02	1.54E-02	0.0968	0.0227	105.97	0.0657
2-6	0.002	0.006	0.0015	V100	966.4	60	1.73E-02	1.60E-02	0.0968	0.0227	102.88	0.0681

Table E2 (Continued)

Chamber (mm * mm)	Radius d (m)	Radius D (m)	Radius (m)	Liquid (name)	Density (kg/m^3)	Tilt (degree)	Velocity (m/s)	Velocity ADJUSTED	Viscosity (Pa.s)	S Tension (N/m)	DCA used	Ca ($\mu v/\gamma$)
2-6	0.002	0.006	0.0015	V100	966.4	80	1.88E-02	1.74E-02	0.0968	0.0227	109.89	0.0743
2-6	0.002	0.006	0.0015	V100	966.4	80	1.92E-02	1.78E-02	0.0968	0.0227	114.33	0.0757
2-6	0.002	0.006	0.0015	V100	966.4	80	2.04E-02	1.89E-02	0.0968	0.0227	122.72	0.0806
2-6	0.002	0.006	0.0015	V100	966.4	80	2.16E-02	1.99E-02	0.0968	0.0227	117.45	0.0850
2-6	0.002	0.006	0.0015	V100	966.4	80	2.40E-02	2.22E-02	0.0968	0.0227	120.63	0.0947
2-6	0.002	0.006	0.0015	V100	966.4	80	2.57E-02	2.38E-02	0.0968	0.0227	108.25	0.1015
2-6	0.002	0.006	0.0015	V100	966.4	80	2.79E-02	2.58E-02	0.0968	0.0227	121.88	0.1099

REFERENCES

Aminzadeh, B., D. A. DiCarlo, and R. Wallach (2011), The Effect of Contact Angle on Saturation Overshoot, *Vadose Zone Journal*, *10*(1), 466–468, doi:10.2136/vzj2010.0047.

Bajpai, A. K., and S. Khandekar (2012), Simulation of Heat Transfer in Liquid Plugs Moving Inside Dry Capillary Tubes, p. 6, Lyon, France. [online] Available from: http://home.iitk.ac.in/~samkhan/Bio_data/publications/Khandekar_Conf_40.pdf

Bian, X., W. W. Schultz, and M. Perlin (2003), Liquid slug motion and contact lines in an oscillatory capillary tube, University of Michigan. [online] Available from: http://www-personal.umich.edu/~schultz/Manuscripts/BianSchultzPerlin.pdf

Bico, J., and D. Quéré (2001), Falling Slugs, *Journal of Colloid and Interface Science*, *243*(1), 262–264, doi:10.1006/jcis.2001.7891.

Bico, J., and D. Quéré (2002), Self-propelling slugs, *Journal of Fluid Mechanics*, *467*, doi:10.1017/S002211200200126X. [online] Available from: http://adsabs.harvard.edu/abs/2002JFM...467..101B (Accessed 30 January 2012)

Blake, T., and J. Haynes (1969), Kinetics of liquidliquid displacement, *Journal of Colloid and Interface Science*, *30*(3), 421–423, doi:10.1016/0021-9797(69)90411-1.

Blake, T. D. (2006), The physics of moving wetting lines., *Journal of Colloid and Interface Science*, *299*(1), 1–13.

Blunt, M., D. Zhou, and D. Fenwick (1995), Three-phase flow and gravity drainage in porous media, *Transport in Porous Media*, *20*(1), 77–103, doi:10.1007/BF00616926.

Bond, R. (1964), The influence of the microflora on the physical properties of soils. II. Field studies on water repellent sands, *Soil Res.*, *2*(1), 123–131.

Brochard-Wyart, F., and P. G. de Gennes (1992), Dynamics of partial wetting, *Advances in Colloid and Interface Science*, *39*(0), 1–11, doi:10.1016/0001-8686(92)80052-Y.

Burlatsky, S. F., G. Oshanin, A. M. Cazabat, and M. Moreau (1996), Microscopic Model of Upward Creep of an Ultrathin Wetting Film, *Phys. Rev. Lett.*, *76*(1), 86–89, doi:10.1103/PhysRevLett.76.86.

Cherry, B. ., and C. . Holmes (1969), Kinetics of wetting of surfaces by polymers, *Journal of Colloid and Interface Science*, *29*(1), 174–176, doi:10.1016/0021-9797(69)90367-1.

Chuoke, R. L., P. van Meurs, and C. van der Poel (1959), The instability of slow, immiscible, viscous liquid-liquid displacements in permeable media, Trans. Am. Inst. Min. Metall. Pet. Eng., 216, 188– 194.

Clarke, A., T. D. Blake, K. Carruthers, and A. Woodward (2002), Spreading and Imbibition of Liquid Droplets on Porous Surfaces, *Langmuir*, *18*(8), 2980–2984, doi:10.1021/la0117810.

Cox, R. G. (1986), The dynamics of the spreading of liquids on a solid surface. Part 1. Viscous flow, *Journal of Fluid Mechanics*, *168*, 169–194, doi:10.1017/S0022112086000332.

Van Dam, D. B., and C. Le Clerc (2004), Experimental study of the impact of an ink-jet printed droplet on a solid substrate, *Physics of Fluids*, *16*(9), 3403–3414, doi:doi:10.1063/1.1773551.

DiCarlo, D. A. (2007), Capillary pressure overshoot as a function of imbibition flux and initial water content, *Water Resour. Res.*, *43*(8), W08402, doi:10.1029/2006WR005550.

Dussan, E. B. (1979), On the Spreading of Liquids on Solid Surfaces: Static and Dynamic Contact Lines, *Annual Review of Fluid Mechanics*, *11*(1), 371–400, doi:10.1146/annurev.fl.11.010179.002103.

Dussan V., E. B. (1976), The moving contact line: the slip boundary condition, *Journal of Fluid Mechanics*, *77*(04), 665–684, doi:10.1017/S0022112076002838.

Dussan V., E. B., and S. H. Davis (1974), On the Motion of a Fluid-Fluid Interface Along a Solid Surface, *Journal of Fluid Mechanics*, *65*(01), 71–95, doi:10.1017/S0022112074001261.

De Gennes, P. G. (1985), Wetting: statics and dynamics, *Rev. Mod. Phys.*, *57*(3), 827–863, doi:10.1103/RevModPhys.57.827.

Extrand (2007), Retention Forces of a Liquid Slug in a Rough Capillary Tube with Symmetric or Asymmetric Features, *Langmuir*, *23*(4), 1867–1871, doi:10.1021/la0625289.

Fermigier, M., and P. Jenffer (1991), An experimental investigation of the dynamic contact angle in liquid-liquid systems, *Journal of Colloid and Interface Science*, *146*(1), 226–241, doi:10.1016/0021-9797(91)90020-9.

Glass, R. J., T. S. Steenhuis, and J.-Y. Parlange (1989), Wetting front instability: 2. Experimental determination of relationships between system parameters and two-dimensional unstable flow field behavior in initially dry porous media, *Water Resources Research*, *25*(6), 1195–1207, doi:10.1029/WR025i006p01195.

Hansen, R., and T. Toong (1971a), Dynamic contact angle and its relationship to forces of hydrodynamic origin, *Journal of Colloid and Interface Science*, *37*(1), 196–207, doi:10.1016/0021-9797(71)90280-3.

Hansen, R., and T. Toong (1971b), Interface behavior as one fluid completely displaces another from a small-diameter tube, *Journal of Colloid and Interface Science*, *36*(3), 410–413, doi:10.1016/0021-9797(71)90014-2.

Hill, D. E., and J.-Y. Parlange (1972), Wetting Front Instability in Layered Soils, *Soil Science Society of America Journal*, *36*(5), 697–702, doi:10.2136/sssaj1972.03615995003600050010x.

Hillel, D., and R. S. Baker (1988), A descriptive theory of fingering during infiltration into layered soils, *Soil Science*, *146*(1), 51–56, doi:10.1097/00010694-198807000-00008.

Hoffman, R. L. (1975), A study of the advancing interface. I. Interface shape in liquid—gas systems, *Journal of Colloid and Interface Science*, *50*(2), 228–241, doi:10.1016/0021-9797(75)90225-8.

Huh, C., and L. Scriven (1971), Hydrodynamic model of steady movement of a solid/liquid/fluid contact line, *Journal of Colloid and Interface Science*, *35*(1), 85–101, doi:10.1016/0021-9797(71)90188-3.

Huh, C., and S. Mason (1977), The steady movement of a liquid meniscus in a capillary tube, *J. Fluid Mech*, *81*(part 3), 401–419.

Jarvis, N. J. (2007), A review of non-equilibrium water flow and solute transport in soil macropores: principles, controlling factors and consequences for water quality, *European Journal of Soil Science*, *58*(3), 523–546, doi:10.1111/j.1365-2389.2007.00915.x.

Jarvis, N. J., P.-E. Jansson, P. E. Dik, and I. Messing (1991), Modelling water and solute transport in macroporous soil. I. Model description and sensitivity analysis, *Journal of Soil Science*, *42*(1), 59–70, doi:10.1111/j.1365-2389.1991.tb00091.x.

Jiang, T.-S., O. . Soo-Gun, and J. C. Slattery (1979), Correlation for dynamic contact angle, *Journal of Colloid and Interface Science*, *69*(1), 74–77, doi:10.1016/0021-9797(79)90081-X.

Lee, P.-S., S. V. Garimella, and D. Liu (2005), Investigation of heat transfer in rectangular microchannels, *International Journal of Heat and Mass Transfer*, *48*(9), 1688–1704, doi:10.1016/j.ijheatmasstransfer.2004.11.019.

Legait, B., and P. Sourieau (1985), Effect of geometry on advancing contact angles in fine capillaries, *Journal of Colloid and Interface Science*, *107*(1), 14–20, doi:10.1016/0021-9797(85)90144-4.

Liu, Y., J.-Y. Parlange, T. S. Steenhuis, and R. Haverkamp (1995), A Soil Water Hysteresis Model for Fingered Flow Data, *Water Resources Research*, *31*(9), 2263, doi:10.1029/95WR01649.

Lowry, T. H. (1997), Removing Silicone Grease from Glassware, *J. Chem. Educ.*, *74*(7), 841, doi:10.1021/ed074p841.

Lunati, I., and D. Or (2009), Gravity-driven slug motion in capillary tubes, *Physics of Fluids*, *21*(5), 052003, doi:10.1063/1.3125262.

Ngan, C. G., and E. B. Dussan V. (1982), On the Nature of the Dynamic Contact Angle: An Experimental Study, *Journal of Fluid Mechanics*, *118*, 27–40, doi:10.1017/S0022112082000949.

Ngan, C. G., and E. B. Dussan V. (1989), On the dynamics of liquid spreading on solid surfaces, *Journal of Fluid Mechanics*, *209*, 191–226, doi:10.1017/S0022112089003071.

Nieminen, J. A., D. B. Abraham, M. Karttunen, and K. Kaski (1992), Molecular dynamics of a microscopic droplet on solid surface, *Phys. Rev. Lett.*, *69*(1), 124–127, doi:10.1103/PhysRevLett.69.124.

Parlange, J.-Y., and D. Hill (1976), Theoretical Analysis of Wetting Frong Instability in Soils, *Soil Science October 1976*, *122*(4), 236–239.

Raats, P. a. C. (1973), Unstable Wetting Fronts in Uniform and Nonuniform Soils, *Soil Science Society of America Journal*, *37*(5), 681–685, doi:10.2136/sssaj1973.03615995003700050017x.

Ralston, J., M. Popescu, and R. Sedev (2008), Dynamics of Wetting from an Experimental Point of View, *Annual Review of Materials Research*, *38*(1), 23–43, doi:10.1146/annurev.matsci.38.060407.130231.

Rose, W., and R. W. Heins (1962), Moving interfaces and contact angle rate-dependency, *Journal of Colloid Science*, *17*(1), 39–48, doi:10.1016/0095-8522(62)90074-0.

Saffman, P. G., and G. Taylor (1958), The Penetration of a Fluid into a Porous Medium or Hele-Shaw Cell Containing a More Viscous Liquid, *Proc. R. Soc. Lond. A*, *245*(1242), 312–329, doi:10.1098/rspa.1958.0085.

Selker, J. S., T. S. Steenhuis, and J.-Y. Parlange (1992), Wetting Front Instability in Homogeneous Sandy Soils under Continuous Infiltration, *Soil Science Society of America Journal*, *56*(5), 1346–1350, doi:10.2136/sssaj1992.03615995005600050003x.

Senn, P. (2007), Spotting of Colloidal Particles, 18 July. [online] Available from: http://www.lbb.ethz.ch/Publications/Diploma_semester_works/Spotting_Colloidal_Particles_PhilippSenn.pdf

Shang, J., M. Flury, J. B. Harsh, and R. L. Zollars (2008), Comparison of different methods to measure contact angles of soil colloids, *Journal of Colloid and Interface Science*, *328*(2), 299–307, doi:10.1016/j.jcis.2008.09.039.

Da Silva, D. L., C. J. L. Hermes, C. Melo, J. M. Gonçalves, and G. C. Weber (2009), A study of transcritical carbon dioxide flow through adiabatic capillary tubes, *International Journal of Refrigeration*, *32*(5), 978–987, doi:10.1016/j.ijrefrig.2008.10.010.

Spildo, K., and J. S. Buckley (1999), Uniform and mixed wetting in square capillaries, *Journal of Petroleum Science and Engineering*, *24*(2–4), 145–154, doi:10.1016/S0920-4105(99)00038-8.

Stadler, Mondon, and Ziegler (2003), Protein adsorption on surfaces: dynamic contact-angle (DCA) and quartz-crystal microbalance (QCM) measurements, *Analytical and Bioanalytical Chemistry*, *375*(1), 53–61, doi:10.1007/s00216-002-1664-5.

Starr, J. L., H. C. DeRoo, C. R. Frink, and J.-Y. Parlange (1978), Leaching Characteristics of a Layered Field Soil, *Soil Science Society of America Journal*, *42*(3), 386–391, doi:10.2136/sssaj1978.03615995004200030002x.

Stroup, W. H., R. W. Dickerson, and R. B. Read (1969), Two-Phase Slug Flow Heat Exchanger for Microbial Thermal Inactivation Research, *Appl Microbiol*, *18*(5), 889–892.

Taha, T., and Z. F. Cui (2006), CFD modelling of slug flow inside square capillaries, *Chemical Engineering Science*, *61*(2), 665–675, doi:10.1016/j.ces.2005.07.023.

Tanner, L. H. (1979), The spreading of silicone oil drops on horizontal surfaces, *Journal of Physics D: Applied Physics*, *12*(9), 1473–1484, doi:10.1088/0022-3727/12/9/009.

Thompson, P. A., and M. O. Robbins (1989), Simulations of contact-line motion: Slip and the dynamic contact angle, *Phys. Rev. Lett.*, *63*(7), 766–769, doi:10.1103/PhysRevLett.63.766.

Tsai, T. M., and M. J. Miksis (1994), Dynamics of a Drop in a Constricted Capillary Tube, *Journal of Fluid Mechanics*, *274*, 197–217, doi:10.1017/S0022112094002090.

Velzenberger, E., K. E. Kirat, G. Legeay, M.-D. Nagel, and I. Pezron (2009), Characterization of biomaterials polar interactions in physiological conditions using liquid–liquid contact angle measurements: Relation to fibronectin adsorption, *Colloids and Surfaces B: Biointerfaces*, *68*(2), 238–244, doi:10.1016/j.colsurfb.2008.10.022.

Voinov, O. V. (1977), Hydrodynamics of wetting, *Fluid Dynamics*, *11*(5), 714–721, doi:10.1007/BF01012963.

Zhang, J., and B. J. Balcom (2010), Magnetic resonance imaging of two-component liquid-liquid flow in a circular capillary tube, *Phys. Rev. E*, *81*(5), 056318, doi:10.1103/PhysRevE.81.056318.